2017

Flow Stress and Microstructure Evolution During Hot Forging of AA6099

Mohammed Tariq Alamoudi
Lehigh University

Flow Stress and Microstructure Evolution During Hot Forging of AA6099

by

Mohammed Tariq Alamoudi

A Thesis

Presented to the Graduate and Research Committee

of Lehigh University

in Candidacy for the Degree of

Master of Science

in
Materials Science and Engineering

Lehigh University

June 2017

Thesis is accepted and approved in partial fulfillment of the requirements for the Master of Science in Materials Science and Engineering Department.

Flow Stress and Microstructure Evolution During Hot Forging of AA6099
Mohammed T. Alamoudi

Date Approved

Thesis Advisor: Prof. Wojciech Z. Misiolek

Associated Chairperson of Department: Prof. Sabrina Jedlicka

ACKNOWLEDGMENTS

In the beginning, I would like to thank ALLAH for providing me with physical and mental strength to continue this work and accomplish a master degree from a recognized department in Lehigh University. I would like to thank my beloved parents for their moral and emotional support and encourage me to continue my study. Especial thanks to my lovely wife Afnan for her patience all the time and for relieving my stresses.

I would like to express my gratitude to my advisor Professor Wojciech Misiolek for accepting me as a member in his distinguished Lowey Institute group and for his continues encouragement and assistance throughout my master degree to make this happen. Also, I would like to thank our former post-doc Dr. Ahmad Chamanfar for helping me in the beginning of this research as well Dr. Nicholas Nanninga and Andrew Layer form Accuride Wheel End Solutions Company for the regular useful discussion. Many thanks to my colleagues in Lowey Institute for all the fun time and technical discussion. I appreciate the help from all the staff in Whitaker lab who eased my study. Moreover, thanks to my friend Sultan Althahban for helping me since I arrived at USA in and outside the university.

Finally, an extended thanks to Accuride Wheel End Solutions Company for funding this research. Also, I'm grateful to my employer King Abdulaziz City for Science and Technology (KACST) for providing the financial support that was essential to complete my Master of Science Degree in the Materials Science and Engineering Department at Lehigh University.

TABLE OF CONTENTS

LIST OF TABLES

LIST OF FIGURES

1 ABSTRACT

Hot forgoing processes are used for plastic deformation of metals at temperatures above the material recrystallization temperature. In this process metal ingots are converted into complex shapes by applying stresses above the yield stress of the deformed material on pre-heated metals in a short period of time. Hot forging process provides products with high strength due to grains refinement and absence of porosity. In the recent years, the demand of aluminum forged products has increased comparing with the cast products, largely in the automotive industry. Many materials characteristics such as: good mechanical properties, low weight, good corrosion resistance, low forging pressure and an ability to be forged into complex shapes make forged aluminum alloys favorable in automotive industry. [1] Because of that, a good understanding of the hot deformation behavior and microstructural evolution are important in a design of the optimized hot forging processes.

The objective of this research is to determine the flow stress behavior and microstructure evolution of newly developed aluminum alloy AA 6099 used in the closed die forging process for truck automotive wheels. As a part of physical process simulation Gleeble hot compression tests were performed at strain rates of 0.01, 0.1 and 1 s^{-1} and temperatures of 350, 400, 450 and 500 ˚C up to a strain of 0.8. The flow stress value is dependent on the deformation temperature, strain, and strain rate and the test parameters were selected in such a way to simulate industrial conditions. The flow stress decreases with increasing deformation temperature and/or decreasing the strain rate. Light Optical Microscopy (LOM), Electron Backscatter Diffraction (EBSD) and microhardness investigations were performed on the hot deformed samples. They revealed that material softening is a result of dynamic recovery and/or partial dynamic

recrystallization at temperature of 350 ºC. Also, after solution heat treatment of the hot deformed samples, there was some evidence of static recrystallization and grain growth.

2 INTRODUCTION

2.1 Forging Background

2.1.1 Hot Forging Process Fundamental

Forging is one of the oldest metal forming processes. It has been known since the prehistoric period, when the hammering was used to form tools. For example, Figure 1 shows the steps to produce a knife by forging. Basically, in forging, the billet should be in solid state and rest between dies where severe force is applied to tooling to plastically deform the workpiece into the desired shape. First, billet is a cut of materiel in a square or circular cross section that will be forged. A die (tool) consists of two parts, upper and lower die, with mating surfaces in the process of hammering or pressing. When both upper and lower parts meet together they do form a die cavity. This cavity is of the shape of the final product for this particular forging step. As seen in Figure 1 more than one step is required to forge the final product.

Figure 1 Schematic illustration of the steps involved in forging a knife. Courtesy of the Mundial LLC and Manufacturing, Engineering & Technology, Fifth Edition. [2]

Forging processes enhance the mechanical properties of the produced parts and in general reduce the waste materials comparing to casting processes. Forging processes are classified based on the temperature of the workpiece or the arrangement of the dies. [3]

Classification of forging processes based on the workpiece temperature divides them to hot forging, cold forging and warm forging.

In hot forging the metal is kept above its recrystallization temperature, relatively about 0.7 of the melting temperature measured in degrees K. At cold forging, the material is at room temperature or slightly higher but always below recrystallization temperature. While warm forging, the temperature is between hot and cold forging temperatures, relatively is about 0.5 of the melting point. Table 1 compares hot, cold and warm forging.

Table 1 Comparison of hot, cold and warm forging [4]

	HOT FORGING	**COLD FORGING**	**WARM FORGING**
TOLERANCES	IT 12 - IT 16	IT 7 - IT 11	IT 9 - IT 12
WEIGHT OF THE WORKPIECE	5 g – 1500 kg	1 g – 50 kg	100 g – 50 kg
SHAPE	any, without undercut	mainly rota-symmetrical, without undercut	rota-symmetrical desirable, without undercut
FORGEABILITY	normally no limit	least forgeability	in between
SURFACE QUALITY	limited	appropriate	advantageous
INTERMEDIATE TREATMENT	not necessary	annealing	normally no surface treatment
DIE LIFE	2000 – 5000 workpieces	20000 – 50000 workpieces	10000 – 20000 workpieces

Note: International Tolerance (IT) shows the precision needed or can be accomplished by each forging process; i.e. hot forging requires generous tolerance, but in cold forging tight tolerance can be achieved on the workpieces. These ITs can be calculated with special formula.

The other classification is based on the arraignment of the dies. The most common types of forging are: open die forging, closed die forging and impression die forging.

Open die forging is the simplest forging process where two flat dies hammer the workpiece to reduce its height, as presented in Figure 2. In closed die forging, the

workpiece is compressed between two dies to fill the cavity without any materials waste (flash), see Figure 3a. In the impression die forging, some flash forms and it's a type of closed die forging, as it is presented in Figure 3b. Table 2 summarizes the advantages and the limitations of both open and closed die forging.

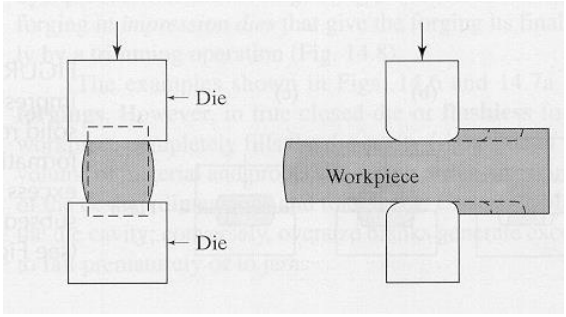

Figure 2 Open die forging [2]

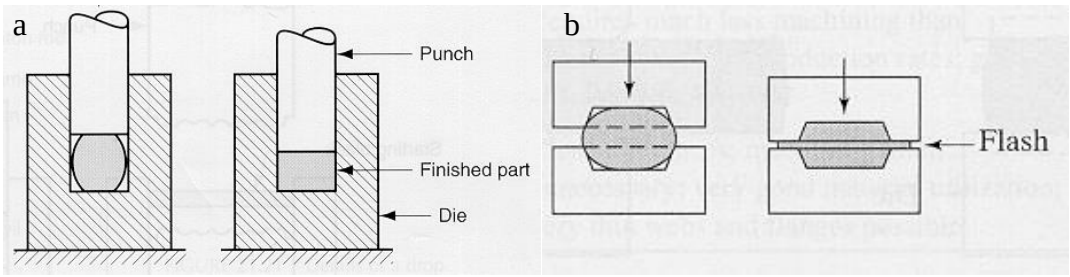

Figure 3 Closed die forging; a) closed die forging b) impression die forging [2]

Table 2 Summary of the advantages and limitations of the open and closed dies forging processes.[2]

Process	**Advantages**	**Limitations**
Open die	Simple, inexpensive dies; wide range of sizes; good strength	Simple shapes only; difficult to hold close tolerances; machining necessary; low production rate; poor utilization of material; high skill labor is required
Closed die	Good utilization of material; better properties than open die forging; good dimensional accuracy; high production rate; good reproducibility	High die cost for small quantities; machining often necessary

2.1.2 Aluminum Alloy

Two main classifications of wrought aluminum alloys are: non-heat-treatable alloys and heat-treatable alloys. The non-heat-treatable alloys such as: 1xxx, 3xxx, 4xxx and 5xxx series are strengthened by strain hardening and solid solution. On other hand, the heat-treatable alloys such as: 2xxx, 6xxx and 7xxx are strengthened by precipitation hardening mechanism. Figure 4 summarized the aluminum alloy types including both casting and wrought alloys. Usually, forged parts are used in structural engineering where the elevated strength is needed. Thus, heat treatable aluminum alloys are used to improve their mechanical performance. After the hot forging process is done, the part is cooled down and for non-heat-treatable alloys this is the final step and the desired properties are obtained. However, for the heat-treatable alloys, the forged part will undergo several heat treatment processes to increase its mechanical properties, which will be discussed later. [5]

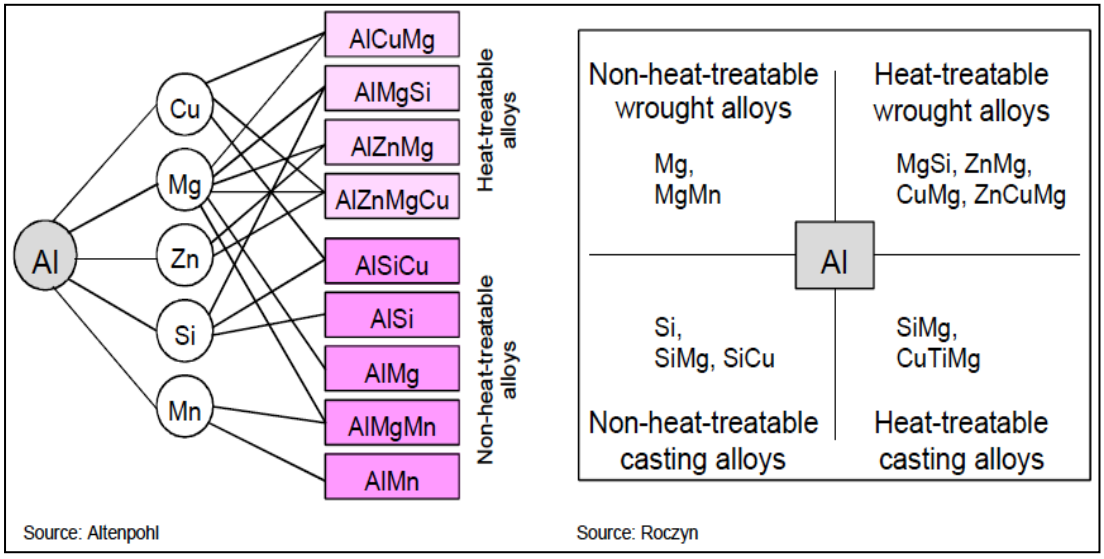

Figure 4 Types of aluminum alloys. [5]

Aluminum alloys are classified depending on the major alloying elements added into aluminum and there are eight (8) different aluminum alloys series from 1xxx to

8xxx. The first digit represents the major allying element has been added. Table 3 summarized all aluminum alloys. The AA6xxx alloys are widely used in automotive industry due to their high forgeability and relatively low flow stress at elevated temperature resulting in satisfactory strength at room temperature at affordable cost.

Table 3. Aluminum alloy groups and major alloying elements. [6]

Group designation	**Major alloying element**
1xxx	Pure aluminum higher than 99 % Al
2xxx	Copper
3xxx	Manganese
4xxx	Silicon
5xxx	Magnesium
6xxx	Magnesium and Silicon
7xxx	Zinc
8xxx	Other elements
9xxx	Unused

Forging products manufactured from aluminum alloys are used in different fields such as: automotive and aerospace industries due to their low weights, high formability, high mechanical properties and good corrosion resistance in comparison with steel. Recently, automotive industries become the highest consumers for aluminum forged products. These products have direct impact on fuel consumption, which then affect the environment. [1] Aluminum products in automotive industry can be found in car chassis, wheels, engines and in suspension systems. For example, Tesla Model S car weighs 185

kg (410 Ibs). The sheet metal and structure components are about 98 % aluminum. [7] Numerous advantages could be achieved by using aluminum forged products in automotive industry such as [6]:

- High corrosion resistance due to formation of thin film of aluminum oxide.
- High specific strength (strength to density ratio).
- Aluminum alloys have relatively low flow stress and are ductile materials, so they require relatively low pressures during forging and high strains are possible.
- During aluminum forging, the microstructure evolution can be controlled and adjusted to the load direction to result in increased fatigue resistance.
- During aluminum forging, the workpiece could be heated near to the die temperature to prevent heat transfer and scale production.

As mentioned before, aluminum alloys are usually forged into parts having different shapes and usages. Each aluminum alloy requires different pressing pressure; depending on many process variables. For instance, the chemical composition of the alloy, the forging method used, the strain rate of the forged part and the temperature of both the workpiece and the die influence forging process and final mechanical properties of the forged parts [8]. Figure 5 shows the flow stress of different aluminum alloys at different stain rates and temperatures compared with the same strain rates and ideal temperature for 1025 carbon steel. At low and medium strength aluminum alloys; i.e. 1100 & 6061, have lower flow stress than 1025 carbon steel, thus they required lower forging pressure. However, higher strength aluminum alloys; i.e. 2014 & 7075, which

belong to the so-called aerospace group of aluminum alloys do require higher pressure than the carbon steel.

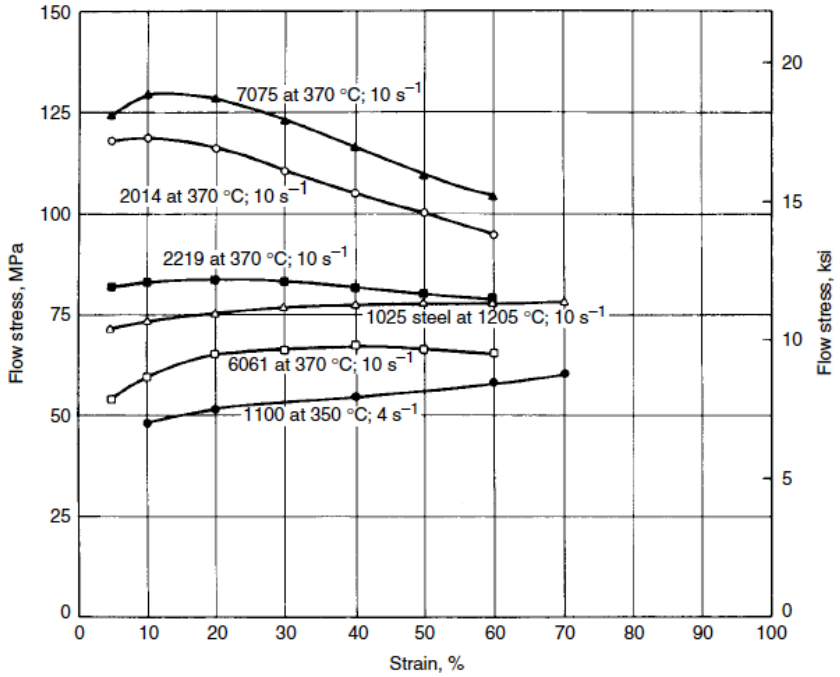

Figure 5 Flow stresses of commonly forged aluminum alloys and of 1025 steel at typical forging temperatures and various levels of total strain. [8]

2.1.3 Forging Aluminum Alloys

Forgeability is defined as the difficulty of achieving specific degrees of deformation in forging without cracking. Also, it is the ability to fill the die. So, metals that can be forged easily with low force have excellent forgeability. In fact, forgeability depends on the type of forging process, the strain rate, the shape complexity (strain), the lubrication as well as the forging and die temperatures. Two tests are common to determine forgeability: upsetting test and hot twist test. In upsetting test, a cylindrical specimen is upset in multiple steps at different temperatures and strain rates until it starts cracking. In the hot twist test, a rod specimen is heated then twisted till failure at various temperatures and strain rates. [9]

Generally, aluminum alloys have high forgeability. Thus, they are suitable for high deformation at few forging steps; usually at one or two steps. The various strength of aluminum alloys made them appropriate for different applications.

In fact, forgeability increases as temperature increases, which is a result of lower flow stress and increased ductility. However, there is a critical temperature above which some other undesirable phenomena occur; such as grain growth or phase melting. In aluminum alloys, the recommended forging temperature window is relatively narrow. Figure 6 shows big differences in forgeability of selected alloys in comparison with other materials representing various families of aluminum alloys. Also, it shows, that for some alloys, a minor increase in forgeability as a result of increasing temperature as in case of AA7xxx.

Figure 7 shows the effect of the strain on the flow stress of AA2014 and 6061 at two different strain rates 10 s^{-1} and 0.1 s^{-1}. As mentioned before the increasing of forging temperature has a direct impact on decreasing the flow stress of an alloy. (See, Figure 8). [8]

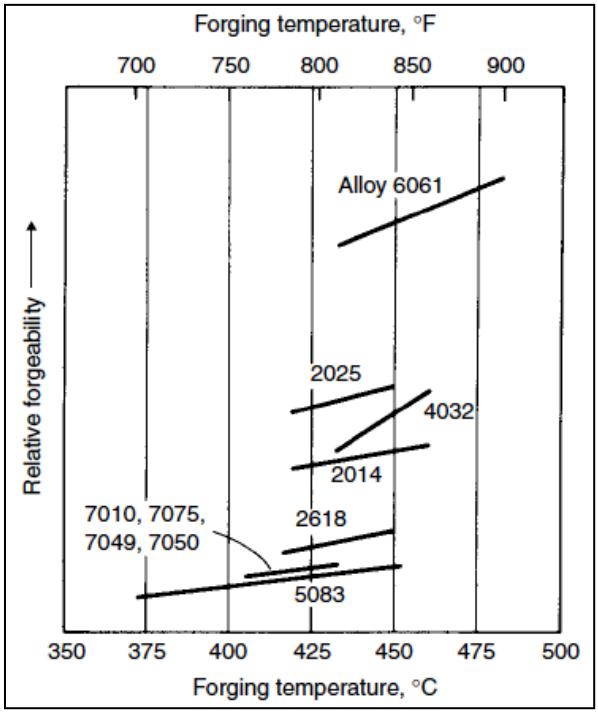

Figure 6 Forgeability vs Forging temperature of different aluminum alloys. [9]

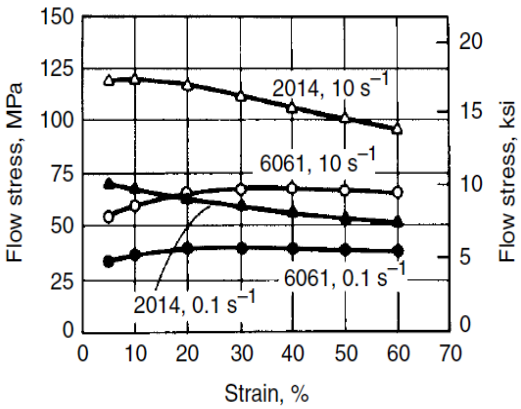

Figure 7 Flow stress of AA6061 & AA2014 at 350 C and different strain rates. [9]

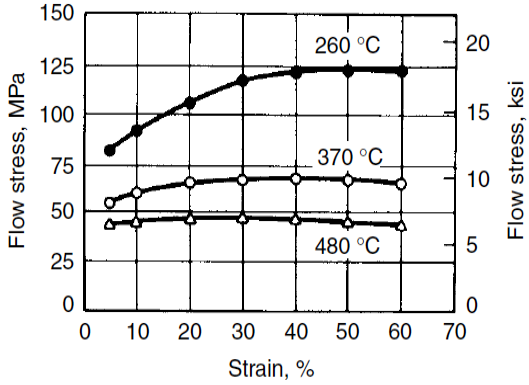

Figure 8 Flow stress of AA6061 at strain rate of 10 s^1 and different temperatures. [9]

From the discussion above, it is clear that temperature has a very serious impact on the forging process. Since the forging temperature in aluminum alloys has narrow window, the billet temperature should be carefully controlled during forging and to be maintained in the recommended temperature range. During aluminum forging process,

the billet will be heated to desired temperature. Then it is forged, usually, by a hydraulic press, which allows long contact time between the billet and the dies. Thus, heat transfers form a workpiece to the colder dies; causing temperature gradient within the workpiece and reduces the surface temperature of the billet. Consequently, the plastic flow at the billet surface is lower than in the billet core. Resulting inhomogeneous plastic flow is called die chilling. To overcome this phenomenon, the isothermal forging process where the dies are heated to the same temperature of the workpiece was proposed.[10]

Isothermal forging process is used for manufacturing of critical and rotating products, especially for aerospace components where near-net-shape is needed to minimize machining. According to the Forging Industry Association., "hot forging is the plastic deformation of metal at a temperature and strain rate such that recrystallization occurs simultaneously with deformation, thus avoiding strain hardening. For this to occur, high workpiece temperature (matching the metal's recrystallization temperature) must be attained throughout the process. A form of hot forging is isothermal forging, where materials and dies are heated to the same temperature. In nearly all cases, isothermal forging is conducted on superalloys in a vacuum or highly controlled atmosphere to prevent oxidation."[11]

Press quenching is another technique used to reduce the distortion of complex geometrical components during heat treatment. In the ideal case, the temperature gradient should be the same at the cross section of the workpiece during quenching. This situation is challenging at big parts with different cross section thickness, e.g. gears. Press quench works by applying controlled force at specific location to hold the component during quenching. The clamps holding the component can work to make quenching process more uniform within the forged components. Press quenching

technique cannot eliminate the temperature gradient but it works to minimize that as much as possible. [12]

2.2 Forged Aluminum Alloy Wheels

2.2.1 Automotive Wheels

For many years steel was the only material used for manufacturing of automotive wheels. However, in the last 100 years, different types of aluminum alloy wheels were developed for this application. For the first time both Daimler-Benz and Auto-Union introduced aluminum wheels in racing cars in the 1930s. Nowadays, more than 50% of automotive wheels are made from aluminum alloys. This is the result of e unique features of aluminum alloys and forged products. As been discussed before, aluminum forged parts are very attractive for automotive industry due their good mechanical properties and reduced weight. [13]

Automotive wheels do require specific mechanical and chemical properties. Structural stiffness and strength are important to carry the car weight and the wheel stiffness depends on the design of the wheel. It should be considered during the wheel design process to achieve required stiffness such as in the steel wheels. Further important aspects are yield strength and fatigue behavior. It's crucial to have the needed strength and fatigue resistance to avoid wheels' deformation and/or failure during service. Also, heat dissipations have direct impact on the wheel and the tire, consequently on the safety of the passengers. So, heat dissipation should be considered to improve the breaking performance and avoid overheating of the tires. In addition, the wheels should have a good corrosion resistance as well as the best dimensional tolerances. [13]

Another important aspect for automotive wheels is their appearance. Many truck drivers expect the wheels to stay shiny and bright for long time in all environmental conditions. Alcoa patented Dura-Bright® technology, which is a surface treatment

penetrating the aluminum and becoming part of the wheel to produce low surface tension on the wheels. It keeps the wheels shiny at any road conditions. This technology prevents the wheel from scratches, cracking, and corrosion counter to conventional coating. [14]

Two most common manufacturing processes used to produce automotive wheels are casting and forging. Cast wheels have lower production cost, but low to moderate fatigue and impact resistance. On the other hand, forged wheels are relatively more expensive but have higher mechanical properties and variety of complex shapes. Usually, cast wheels are used for passenger cars and are most common because they are relatively less expensive than forged wheels. Forged wheels mainly used for trucks and high speed cars where high strength and fatigue resistance are needed. They are much expensive than cast wheels due to the manufacturing process expenses like tooling and equipment.

2.2.2 Manufacturing Process

During hot forging process, a cast and homogenized or already extruded billet of aluminum alloy, usually AA6061, is heated up to around 450-500˚C. Then, the billet is placed in a forging press and forged with high pressure to form the wheel. This deformation step because of proper die design will force the alloy grains to align in such a way to increases the mechanical properties of the forged wheel. The first step is to forge the billet and to change the shape of the cylindrical billet into a shape closed to a final wheel geometry called forged blank. Usually it takes two steps to accomplish that. After this operation, this forged blank will be spun to form the rim of the wheel. Then, some machining operations are performed to obtain the detailed design. At this stage, the forged wheel is having minimal porosity due to heavy deformation. Further heat treatments are performed to enhance the mechanical properties of the wheel. Figure 9 shows typical stages of the wheel forging process.

Figure 9 Forged wheel process [15]

3 Research Objective

The research objective of this study is to investigate the microstructure development during hot forging process and subsequent heat treatment of a newly developed aluminum alloy 6099. The need for understanding of mechanical behavior of new alloy drives the physical modeling of the microstructure evolution during forging process.

4 EXPERIMENTAL PROCEDURE

4.1 Experimental Approach

4.1.1 Material

The aluminum alloy used in the experiments of this investigation was AA6099. This is a newly developed alloy and it was provided by Accuride Wheel End Solutions. Table 6 shows the chemical composition ranges for AA6099. Two different billets; i.e. Lot#1 and Lot#2, with slightly different chemical composition were cast, then homogenized.

Table 4 Chemical composition of AA6099

	Si	**Fe**	**Cu**	**Mn**	**Mg**	**Cr**	**Zn**	**Ti**
AA6099	0.8-1.2	0.7 max	0.1-0.7	0.1-1.2	0.7-1.2	0.04-0.35	0.25	0.1

Some preliminary investigation performed on this new alloy showed the as cast samples have three phases Mg_xSi_y, Al-Fe-Si phase, Cu rich phase as well as transition metals such as Fe, Mn and Cr. On the other hand, during the homogenization of the billet, the Cu rich phase totally dissolves and only two phases were present Mg_xSi_y and Al-Fe-Si. Figure 10 shows the different phases of homogenized AA 6099.

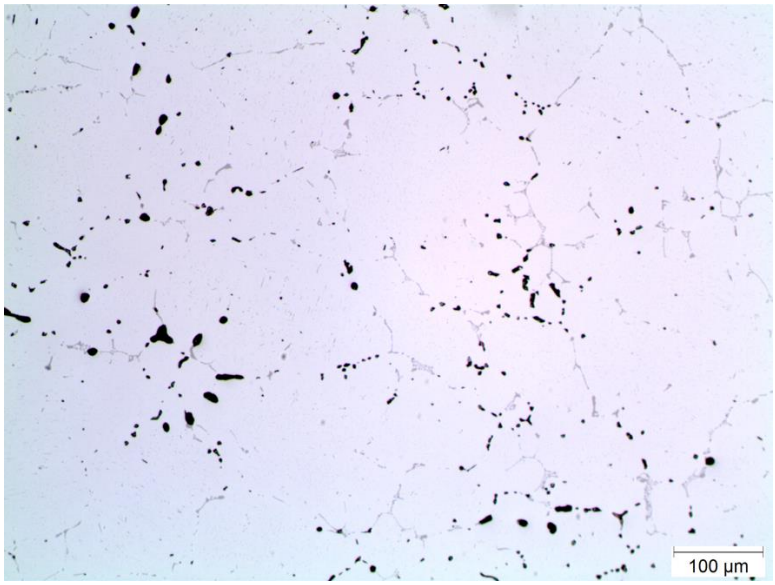

Figure 10 As polished micrograph of AA 6099 after homogenization of Lot#1

In the beginning of studying Al-Mg-Si alloys, it was assumed that Mg_2Si is the only precipitating phase formed.[16] In 1948 Geisler and Hill [17] reported that X-ray Laue pattern zones indicated the formation of other nano phases which are GP zones (Guinier–Preston zones). They are needless with a typical size of (~2×2×10 nm^3) at temperature of 200 ºC. With further heating, the GP zones start to form rods which are called β′. The last phase is the β which has the plate like shape at equilibrium; Mg_2Si.[16]

Recent studies on this subject revealed that the precipitation sequence for 6xxx alloys is: super saturated solid solution →atomic clusters→GP zones→β″→β′/B′→β (stable). So, the first phase start to precipitate is the GP zones where Si/Mg>1 and the morphology is almost spherical with 1-2 nm in size, also called GP-I phase. The next phase is β″, which is Mg_5Si_6. It has fine needles shape with about 4×4×50 nm^3 in size, also called GP-II. Both, GP-I and GP-II, have the highest density in the aluminum matrix, which give it the mechanical strength. The next phase is β′ which has lower

Mg/Si ratio than β, having the formula $Mg_{1.7}Si$. It has ribbon like shape up to few µm long. The last phase is the equilibrium phase which is β (Mg_2Si). It has plate like shape with a diameter up to 20 µm. Table 5 summarize all these phases. [18]

Table 5 Overview of Mg–Si containing phases in 6082 Al-alloys. [18]

Phase	**Formula**	**Unit cell**	**Morphology/typical size**
GP	Si/Mg>1	Unknown	Almost spherical/1–2 nm
β″	Mg_5Si_6	Monoclinic C2/m a= 15.16 Å, b= 4.05 Å c= 6.74 Å, β= 105.3 °	Needles/up to 40 x 40 x 350 $Å^3$
β′	$Mg_{1.7}Si$	Hexagonal a= 7.05 Å, c= 4.05 Å	Ribbons/several µm long
β	Mg_2Si	fcc (CaF-type) a= 6.39 Å	Plates or cubes/up to 10–20 µm diameter
B′	Mg/Si≈1	Hexagonal a= 10.3 Å, c= 4.05 Å	Ribbons/up to 1 µm

The samples used in the experiments were sectioned form the center and mid radius of the homogenized billet and a typical microstructure is shown in Figure 11. This selection was performed to be away from any inverse segregation and to obtain equiaxed grains, as shown in Figure 12.

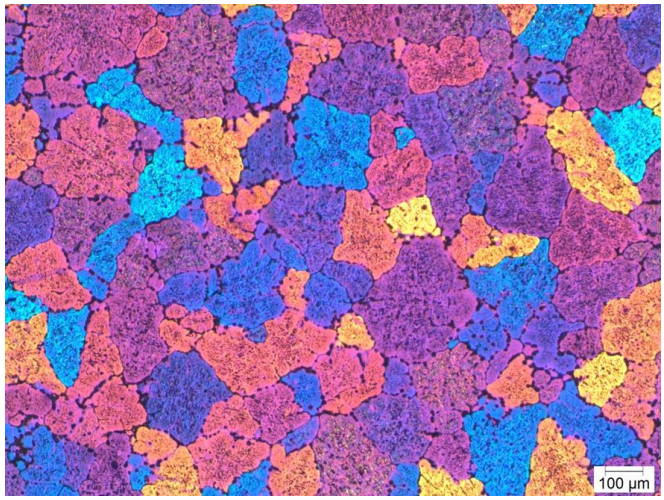

Figure 11 Micrograph shows the equiaxed grains of AA 6099 etched by Barker's after homogenization of Lot#1

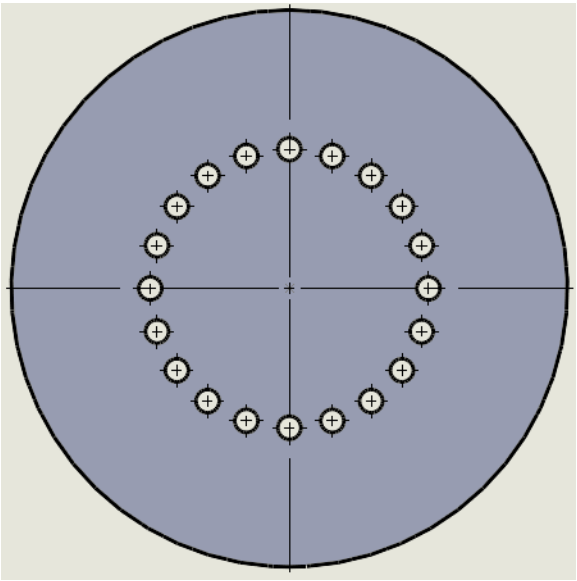

Figure 12 Sketch showing how the samples were located in the center and mid radius of the billet

4.1.2 Experiments

To simulate the forging process and study the flow stress behavior of AA 6099, the samples were deformed in a compression mode by thermomechanical Simulator – Gleeble (model, 3500)® system using the range of temperatures and strain rates corresponding to the industrial practice. Then, the deformed samples were solution heat treated to understand the solution heat treatment effect on microstructure development and mechanical properties. This procedure allowed physical simulation of the entire cycle of the industrial process. All samples were investigated under the Light Optical Microscopy (LOM) to analyze their microstructure. Since the LOM didn't reveal the microstructure very well, some selected samples were investigated more in depth either by Scanning Electron Microscopy (SEM) or by Electron Backscattered Diffraction (EBSD). The EBSD was used to look for any subgrains or recrystallized grains formed and which did not show in the LOM micro-images. In addition, micro-hardness indentation testing (microhardness test) was performed on some deformed samples. The microhardness test shows good strength reference of specific localized area, usually

within a grain, better than tensile test, which shows the average strength of the specimen. In other words, recrystallized grains will show lower hardness reading number comparing with non-recrystallized ones, which have higher dislocation density. [19] Table 6 summarized all samples that have been investigated.

Table 6 Summary of the samples that have been tested

Strain rate s^{-1}	Temperature ºC	LOM	EBSD	Micro-hardness test
0.01	350	√	√	√
	400	√		
	450	√		
	500	√	√	√
0.1	350	√	√	√
	400	√		
	450	√		
	500	√	√	√
1	350	√	√	√
	400	√		
	450	√		
	500	√	√	√

4.2 Dynamic Thermal-Mechanical Testing

4.2.1 Sample Preparation

The cylindrical specimens (coupons) were selected for uniaxial compression test having the height and diameter dimensions of 25.4 mm and 12.7mm, respectively. The flat surface of the test coupon was slightly ground to remove the oxide layer then rinsed with Ethanol. Two thermocouples were welded to the coupons cylindrical surface to

monitor and control the temperature distribution during the tests. One thermocouple was welded in the center of the sample and the other near the edge. The central thermocouple was controlling the desired temperature. The one near the edge was used to ensure monitoring of the temperature and to know the temperature difference between the middle and the edge of the samples. The lubricant used during the Gleeble experiments was flexible graphite sheet. The graphite sheet was cut into circular shape approximately of the same size as the flat surface of the test coupon. Then, it was placed between the both ends of the test coupon and Gleeble jaws by applying slight force toward the coupons inside the Gleeble chamber. Figure 13 shows the entire set up of the sample, lubrication sheet and deformation chamber including quenching nozzles of the Gleeble 3500 thermomechanical simulator.

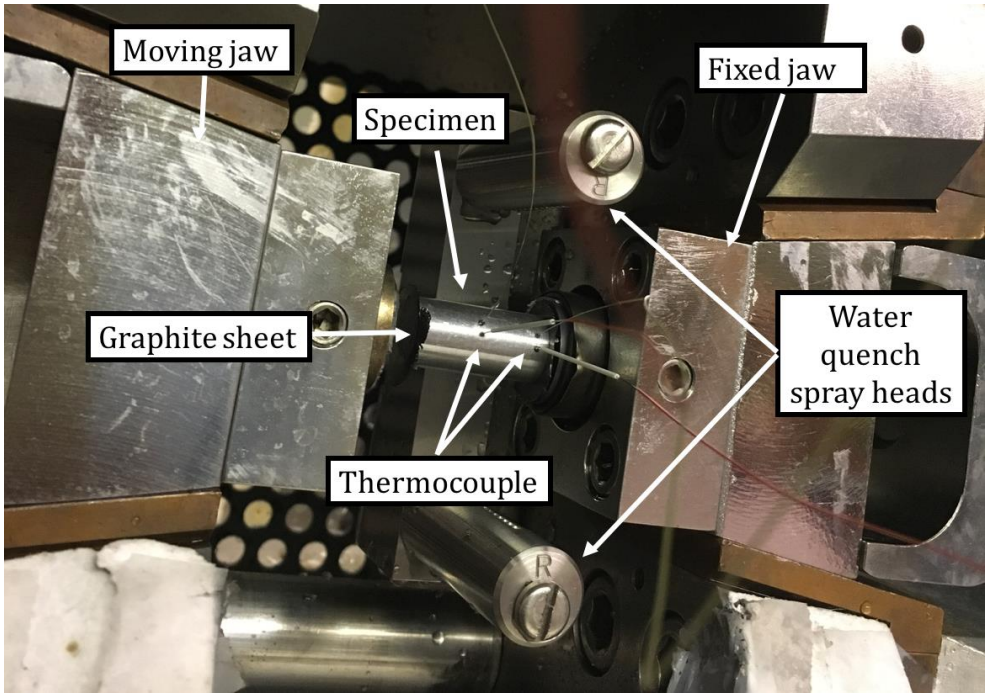

Figure 13 Gleeble experiment set-up

4.2.2 Test Approach

The uniaxial compression tests were conducted on a Gleeble 3500 thermomechanical simulator. In total, 48 compression tests were conducted on both

Lot#1 and Lot#2 following test conditions presented in Table 7. Each deformation condition, combination of temperature and strain rate was performed twice.

Table 7 Deformation Test Conditions

Strain rate s^{-1}	**Deformation Temperature ˚C**
0.01	350
	400
	450
	500
0.1	350
	400
	450
	500
1	350
	400
	450
	500

The samples were heated to the desirable deformation temperature at a heating rate of 10 °C/s and held for 5 min to ensure homogenous temperature distribution through the sample. The temperature was monitored by the two thermocouples. After that, the sample was deformed to a total true strain of 0.8 and then immediately water-quenched by the quenching system inside the Gleeble chamber. The quenching was applied to preserve the developed microstructure as a result of the used deformation conditions and to prevent any static recovery or static recrystallization for the metallographic study.

4.3 Heat Treatment

4.3.1 Sample Preparation

The solution heat treatment experiment has been applied to the hot deformed samples at the lowest and highest temperatures (350 C & 500 ºC) for all strain rate values (0.01, 0.1 and 1 s^{-1}) for Lot#1. Each deformed sample was cut into two halves, where each half contained of four (4) different zones; i.e. surface deformation zone (SDZ), main deformation zone (MDZ), dead metal zone (DMZ) and transition zone (TZ). Then, each half was divided into 4 pieces. So, in total, we had eight (8) pieces from one original sample, see Figure 14.

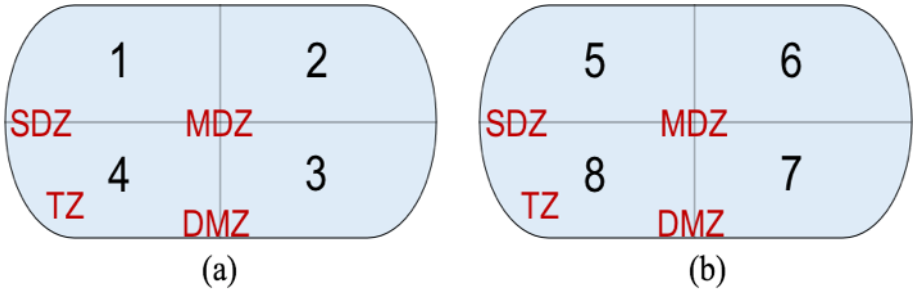

Figure 14 Schematic cross section of the deformed sample showing a typical specimen with approximate position of the characteristic zones; SDZ, MDZ, DMZ and TZ. a) first half & b) second half.

4.3.2 Solution Heat Treatment Approach

In solution heat treatment, five pieces that illustrated in Figure 14 has been used; i.e. pieces # 1, 2, 3, 4 and 5. All pieces were inserted into the furnace before the temperature rose. The furnace was turned on with the heating rate of 10 ºC/min. It required 2 hours to reach the desired temperature, which was 550 ºC (1020 ºF). Then the temperature was held for 45 minuets. The pieces were pulled out the furnace in following order (see Figure 15):

- 1st piece after 40 min
- 2nd piece after 80 min
- 3rd piece after 120 min

- 4th piece after 143 min
- 5th piece after 165 min

Each piece was immediately quenched with water to preserve the microstructure. The reason for having different samples during the solution heat treatment was to understand the microstructure evolution during solution heat treatment.

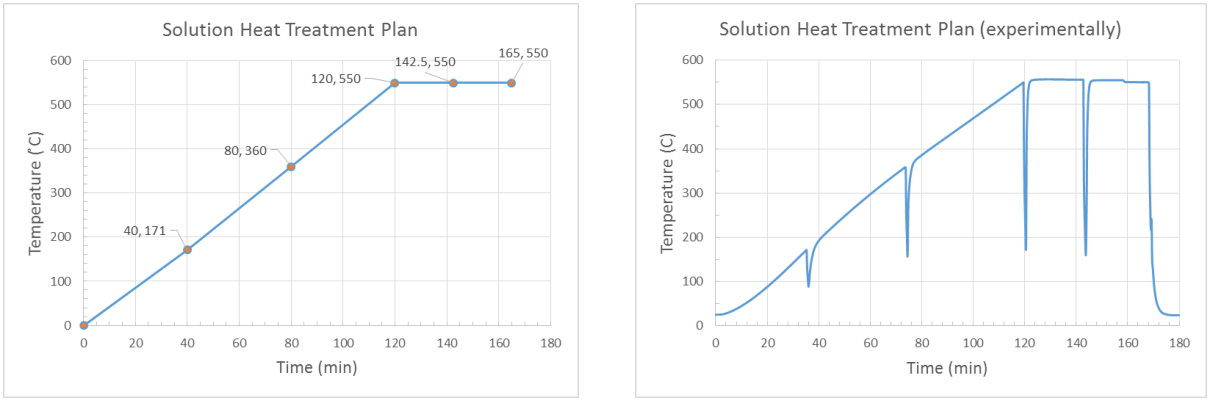

Figure 15 Solution Heat Treatment Plan (on the left) and experimental execution of the plan (on the right)

4.4 Analysis of Experimental Data

4.4.1 Light Optical Microscopy (LOM)

In the beginning, the samples were investigated by Light Optical Microscopy (LOM) to study the microstructure evolution after hot deformation and solution heat treatment. The deformed samples were cut parallel to the deformation axis by abrasive cutting into two halves to examine the four deformed zones shown in Figure 14. However, the solution heat treatment samples, each representing a half of the deformed sample was cut into four pieces using Struers Accutom-50 high speed saw to provide high precision cut. After that, standard metallography procedure was applied as follow:

1- The samples were mounted in Bakelite using Struers ProntoPress-20.

2- Standard grinding procedure using 120, 320, 400 and 600 grit SiC papers, followed by water rinsing was applied.

3- Then polishing using 6 µm diamond and 3 µm, 1 µm and 0.05 µm colloidal silica was done. After each step the samples were rinsed with ethanol and air dried.

After the samples were metallography prepared, they were etched using Keller's (190 mL water, 5 mL HNO_3, 3 mL HCl, 2 mL HF). The samples were immersed with face up in the etchant for approximately 2 – 3 minutes. Then, they were rinsed with water then ethanol and dried with warm air.

The microstructure was studied by Olympus BH2 microscope under different magnifications; 50, 100, 200 and 400x. The images were recorded by attached digital camera PAXcam5 and using Paxit image acquisition software.

4.4.2 Scanning Electron Microscope (SEM) and Electron Backscatter Diffraction (EBSD)

The samples for the SEM analysis were prepared using metallographic standard procedure as described above. In addition, ion milling was used after final polishing with colloidal silica in a vibratory polisher. Due to the softness of the AA6099, it is hard to obtain smooth surface with traditional polishing techniques. Because of that, the Hitachi IM4000 Ion Milling System was used to enhance the polishing quality. After many tries and errors with the ion milling system, the best polishing conditions were established and used. The best-developed parameters of ion milling are listed below:

- Swing angle - 360 º
- Tilt angle - 80 º
- Eccentricity - 5 mm
- Gas flow rate - 0.1 cm^3/min
- Accelerating voltage - 2.5 V
- Time - 15 minutes

Then the samples were coated with Iridium (Ir) to achieve a few Angstroms thick film. This coating is needed to improve the imaging of sample surface. Also, this

technique creates a conductive layer, which prevents charging, reduces thermal damage and improves the secondary electron signal.

For SEM imaging, the backscattered electron (SEM-BSE) technique was used which shows the different elements present in a sample. The setup for SEM-BSE was:

- Accelerating voltage - 10 kV
- Gun Brightness - 3
- Aperture size - 2
- Condense lens – 11 (moderate current flow)

For EBSD analysis the setup was different since more current flow was needed to acquire more signals. Thus, the SEM setup for EBSD analysis was selected as follows:

- Accelerating voltage - 20 kV
- Gun Brightness - 5
- Aperture size - 1
- Condense lens – 1 (high current flow)

4.4.3 Microindentation Hardness Testing

Six (6) as deformed samples under the following conditions: strain rates of 0.01, 0.1 and s-1 for both temperatures 350 and 500 ºC (see Table 5) were micro hardness tested. The samples were metallography prepared as described in section 3.4.1. The microhardness tester that used is Leco LM248AT. An elongated diamond knoop test indenter was used with 25g load and 10 seconds dwell time, see Figure 16. Then the software was used to measures the indents and calculate the indents spacing. The indents were performed are 20 indents along a straight line parallel to the compression direction at the middle of the sample as shown in Figure 17.

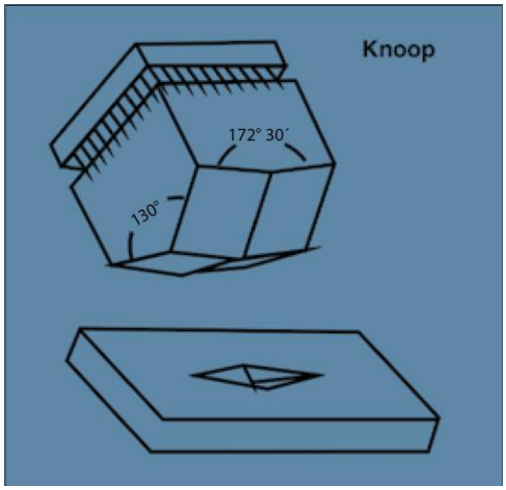

Figure 16 Schematic of the Knoop indenter and the shape of an impression. [20]

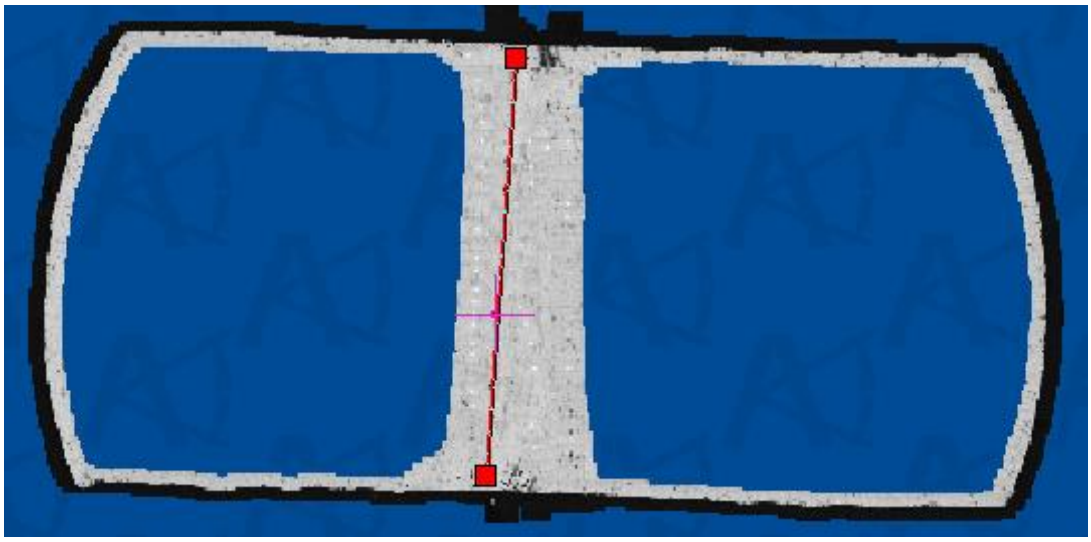

Figure 17 A deformed sample image shows the 20 indents along the red line.

5 RESULTS

5.1 Flow Stress Data

The true stress –true strain curves for hot compression of 6099 aluminum alloy at temperatures of 350, 400, 450 and 500 ºC with different strain rates of 0.01 s^{-1}, 0.1 and 1 s^{-1} are presented in Figure 18. Because each compression test has been performed twice, the average of two tests has been calculated and then plotted as shown in Figure 18.

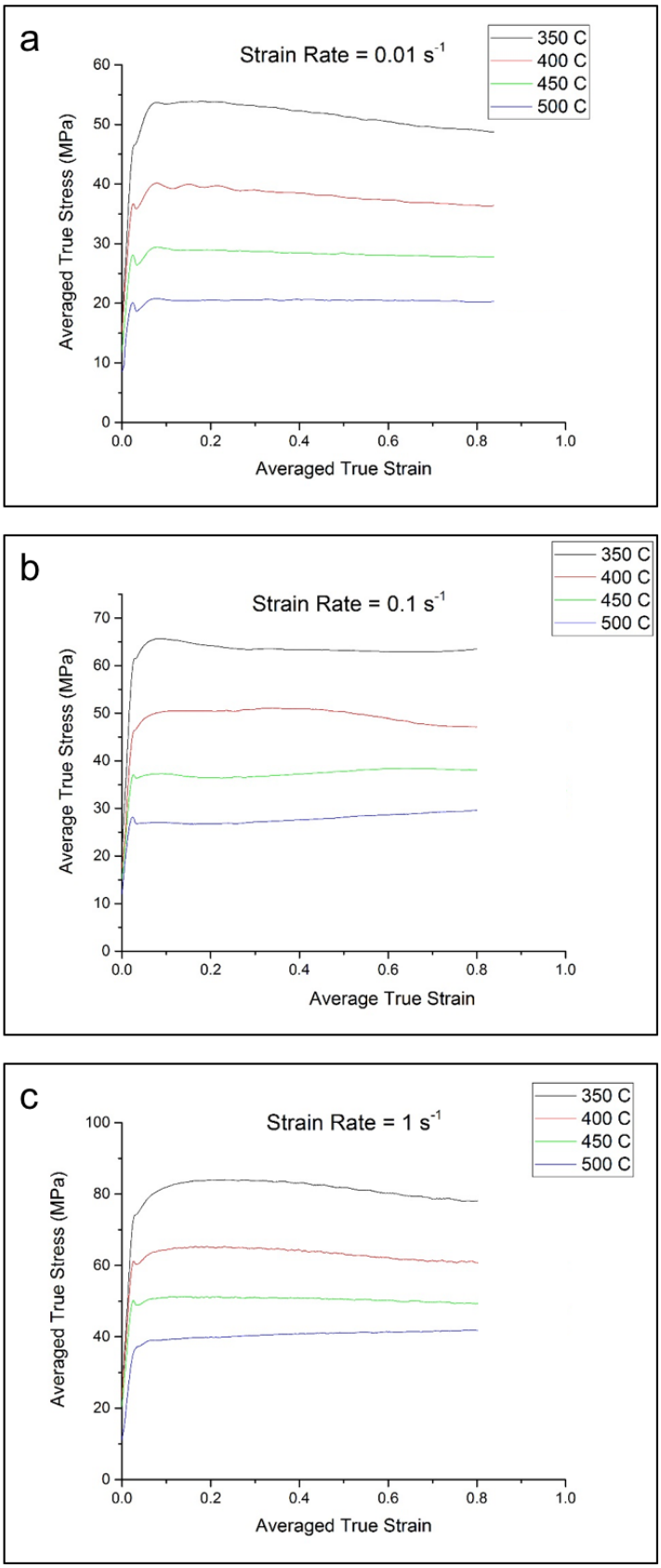

Figure 18 True stress–true strain curves of 6099 alloy during hot compression deformation: (a) = 0.01 s^{-1}; (b) $\dot{\varepsilon}$ = 0.1 s^{-1}; (c) $\dot{\varepsilon}$ = 1 s^{-1}

5.2 LOM Microstructure

5.2.1 Undeformed Samples

The microstructure of undeformed samples for both Lot#1 and Lot#2 were prepared for metallographic analysis as discussed before. In Figure 19, the samples were etched by Barker's reagent; i.e. 2.5% Fluoboric acid in water at 20 V DC, 4 A for 2 minutes. Then, crossed polarized light was used as well as a sensitive tint (λ plate) to obtain needed contrast. In Figure 20, the samples were etched by Keller's reagent; i.e. 190 ml water, 5 ml HNO_3, 3 ml HCl, 2 ml HF.

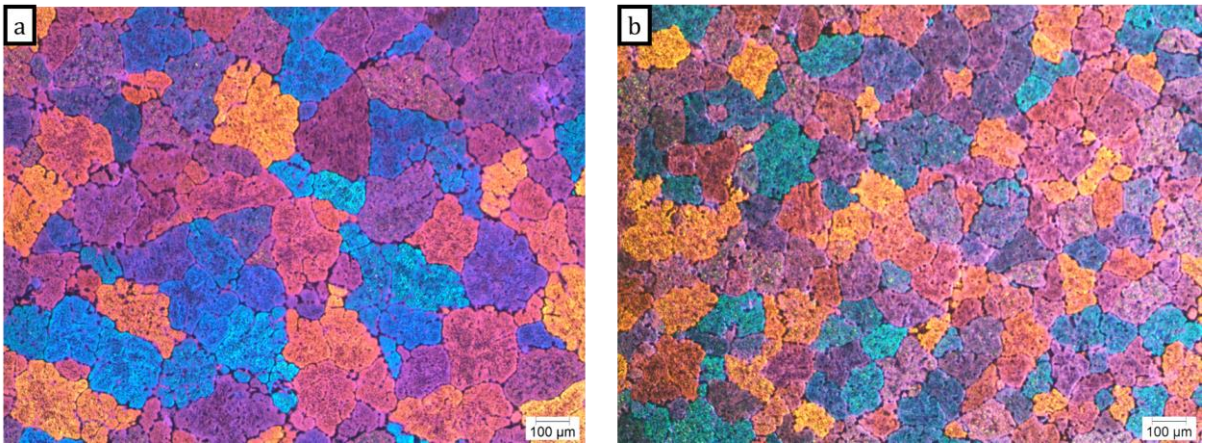

Figure 19 Microstructures of undeformed samples observed in polarized light. a) Lot#1, b) Lot#2.

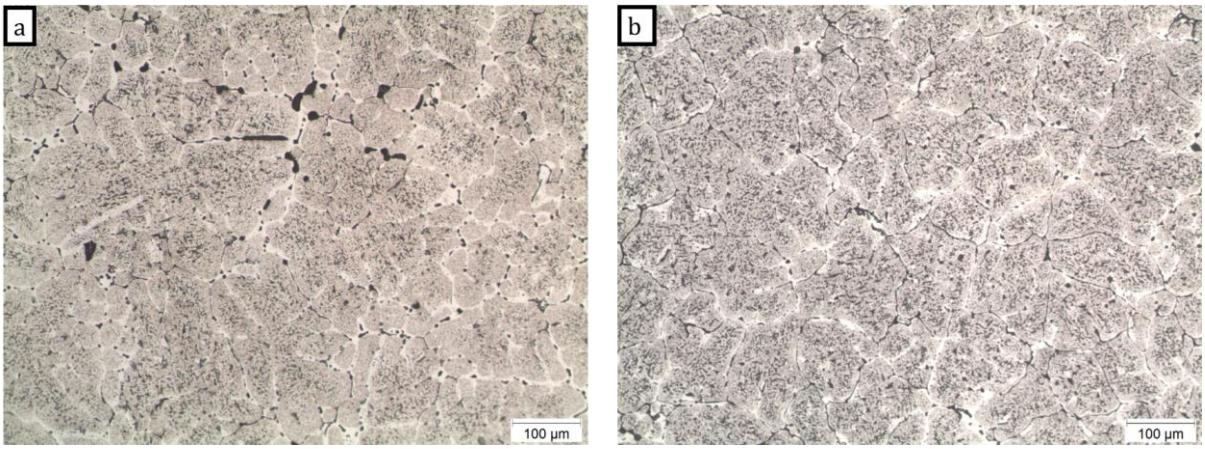

Figure 20 Light optical images of microstructures of undeformed samples. a) Lot#1, b) Lot#2.

5.2.2 Hot Deformed Samples

The hot deformed samples were metallurgy prepared as explained in section 3.4.1 then etched by Keller's reagent. Figure 21 and Figure 22 summarized all the microstructure of hot deformed samples.

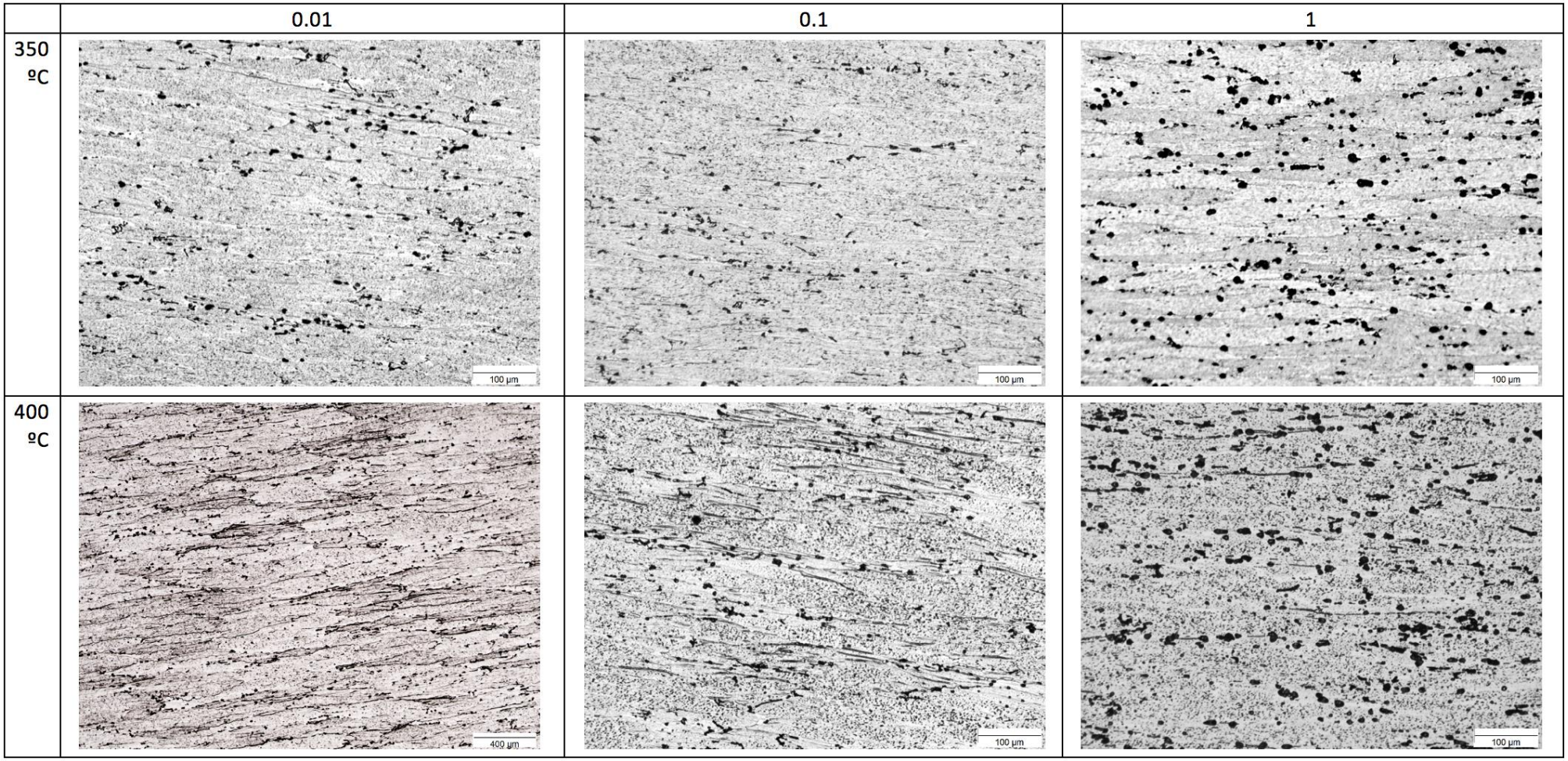

Figure 21 Optical microstructures of deformed samples at temperature of 350 & 400 ºC at strain rates of 0.01, 0.1 and 1 s^{-1}

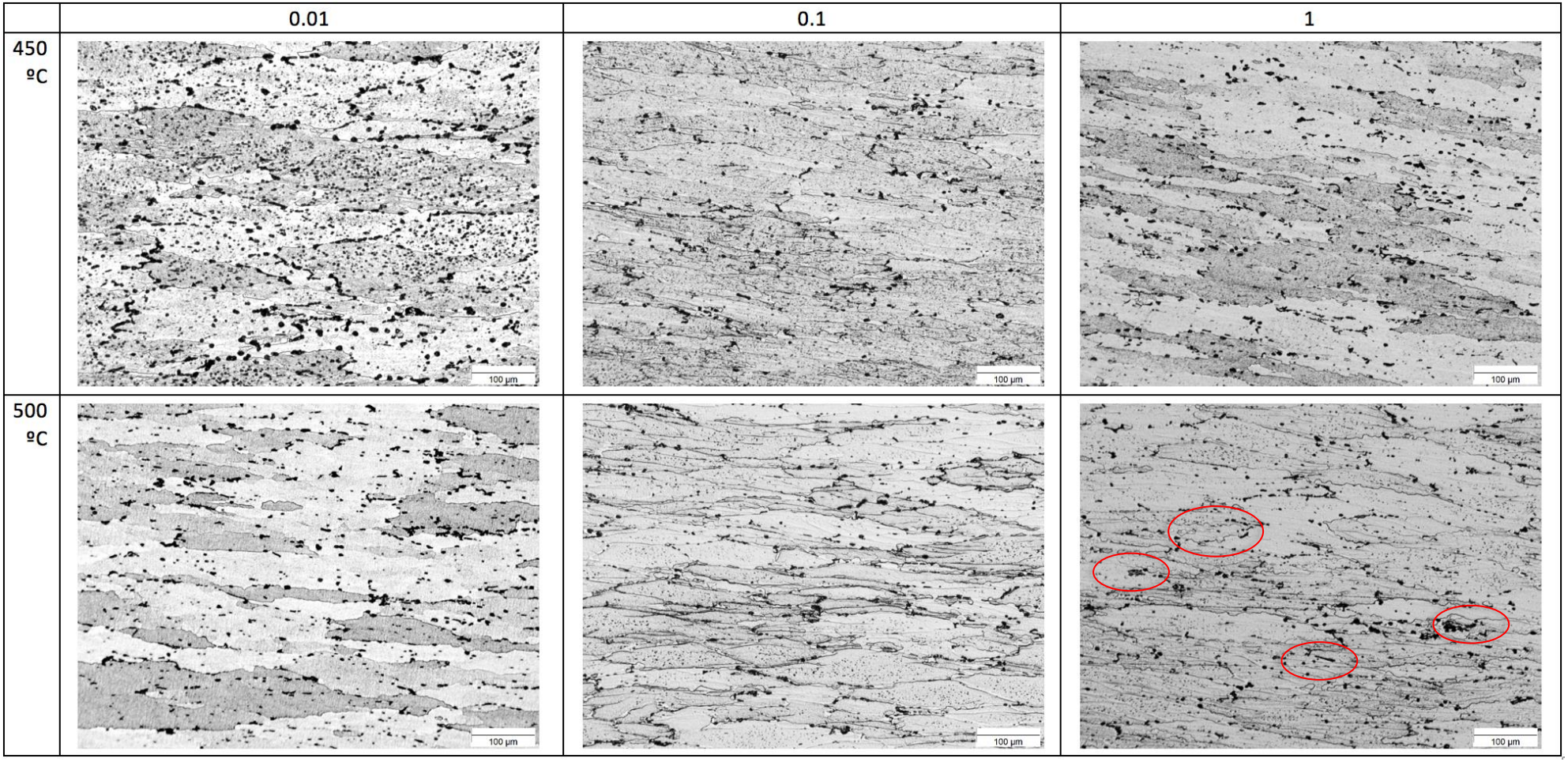

Figure 22 Optical microstructures of deformed samples at temperature of 350 & 400 ºC at strain rates of 0.01, 0.1 and 1 s^{-1}

5.2.3 Solution Heat Treated Samples

In the performed solution heat treatment, the specimens were heated to about 550 ºC. This temperature was enough to dissolve significant amount of the alloying element into the solid solution. Then, the samples were rapidly quenched to room temperature. This created supersaturated solid solution where the alloying elements are in the solution of the matrix phase. [21]

The following figures represent the micrographs for all solution heat treated samples as follow:

- Figure 23 to Figure 30 shows the results of strain rate of 0.01 s^{-1},
- Figure 31 to Figure 34 shows the results of strain rate of 0.1 s^{-1};
- Figure 35 to Figure 42 shows the results of strain rate of 1 s^{-1}.

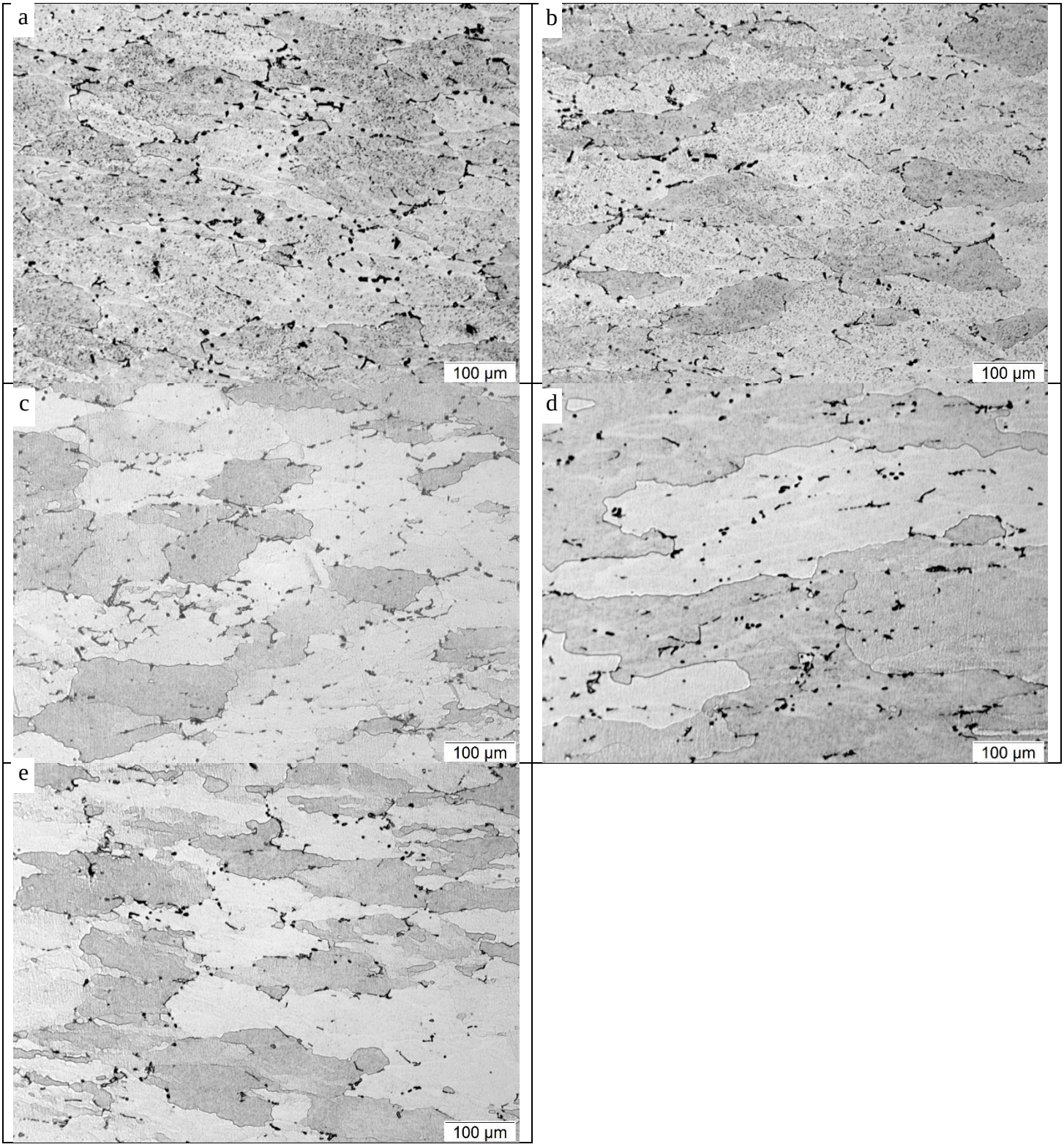

Figure 23 Optical microstructures of solution heat treated samples deformed at temperature of 350 and strain rate of 0.01 s^{-1} at SDZ position. a) after 40 min, b) after 80 min, c) after 120 min, d) after 143 min and e) after 165 min.

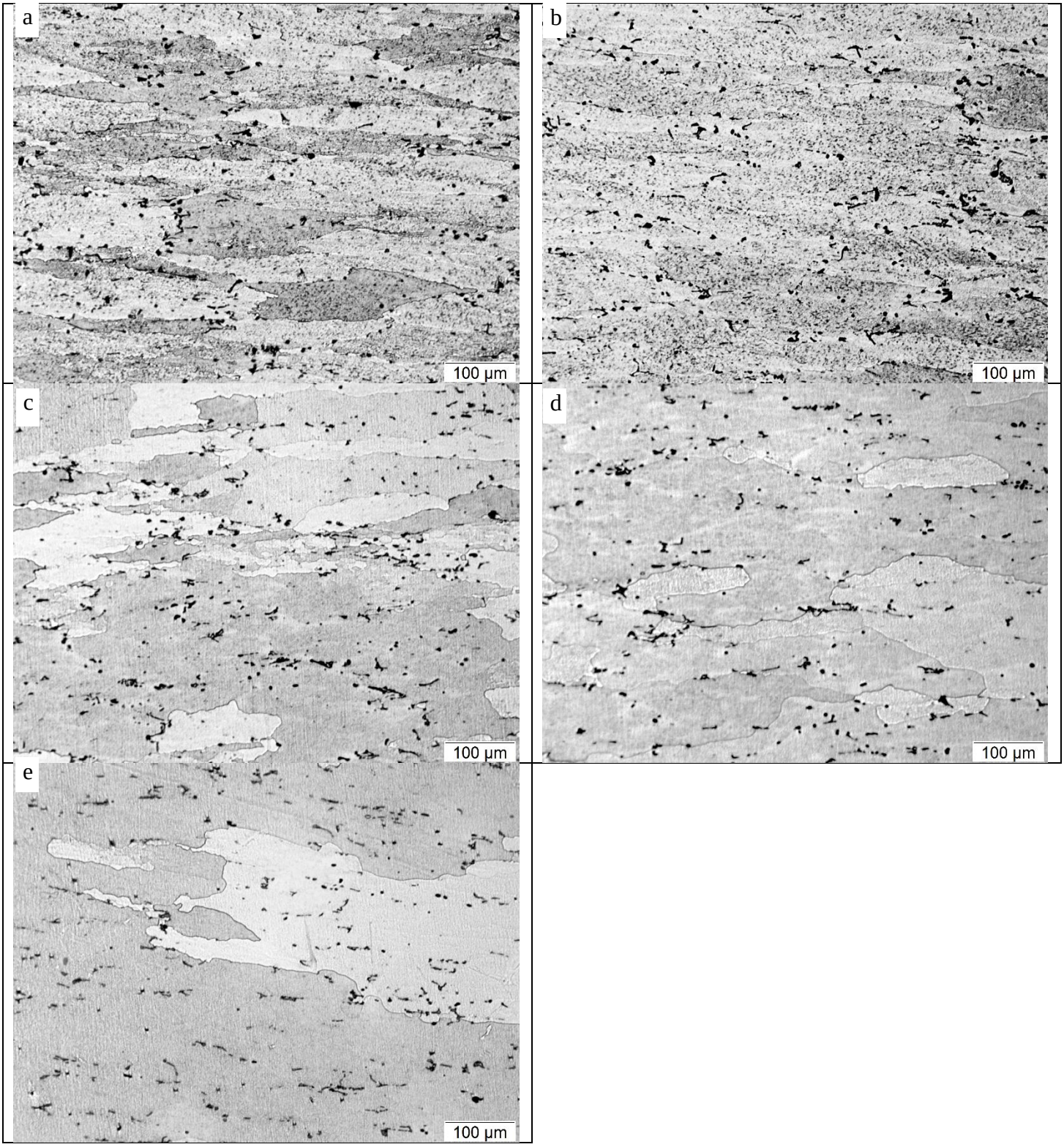

Figure 24 Optical microstructures of solution heat treated samples deformed at temperature of 350 and strain rate of 0.01 s^{-1} at MDZ position. a) after 40 min, b) after 80 min, c) after 120 min, d) after 143 min and e) after 165 min.

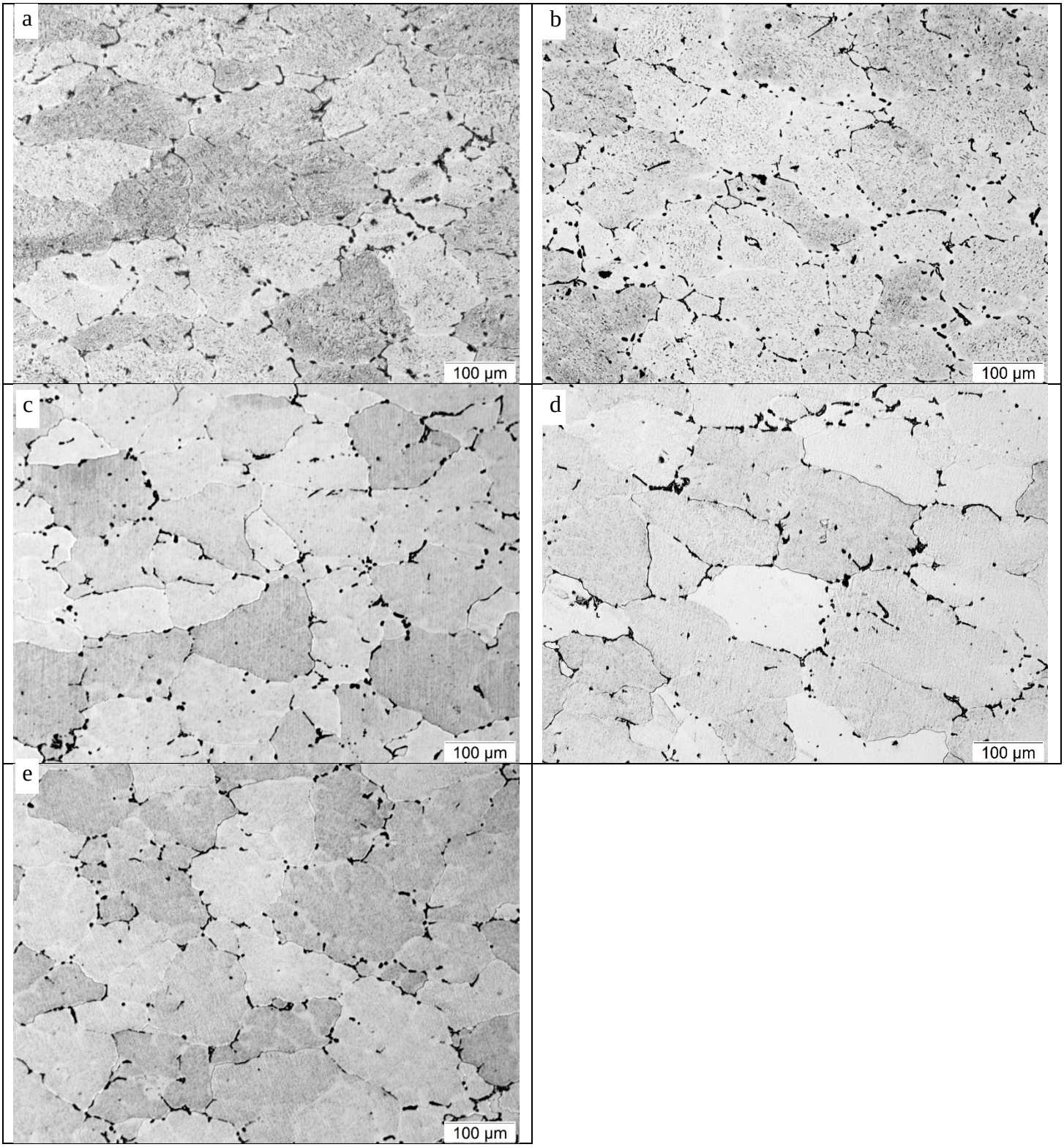

Figure 25 Optical microstructures of solution heat treated samples deformed at temperature of 350 and strain rate of 0.01 s^{-1} at DMZ position. a) after 40 min, b) after 80 min, c) after 120 min, d) after 143 min and e) after 165 min.

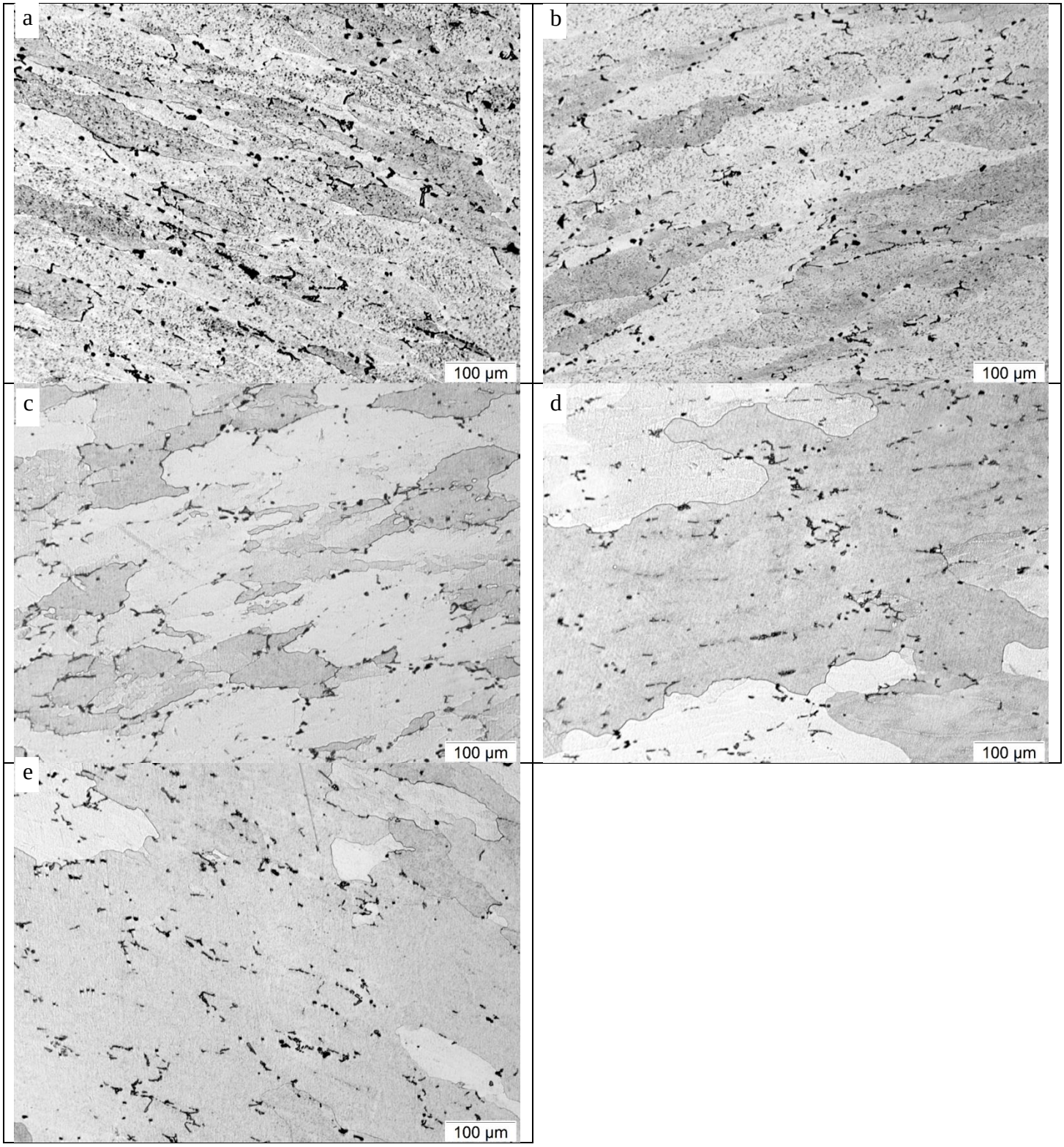

Figure 26 Optical microstructures of solution heat treated samples deformed at temperature of 350 and strain rate of 0.01 s^{-1} at TZ position. a) after 40 min, b) after 80 min, c) after 120 min, d) after 143 min and e) after 165 min.

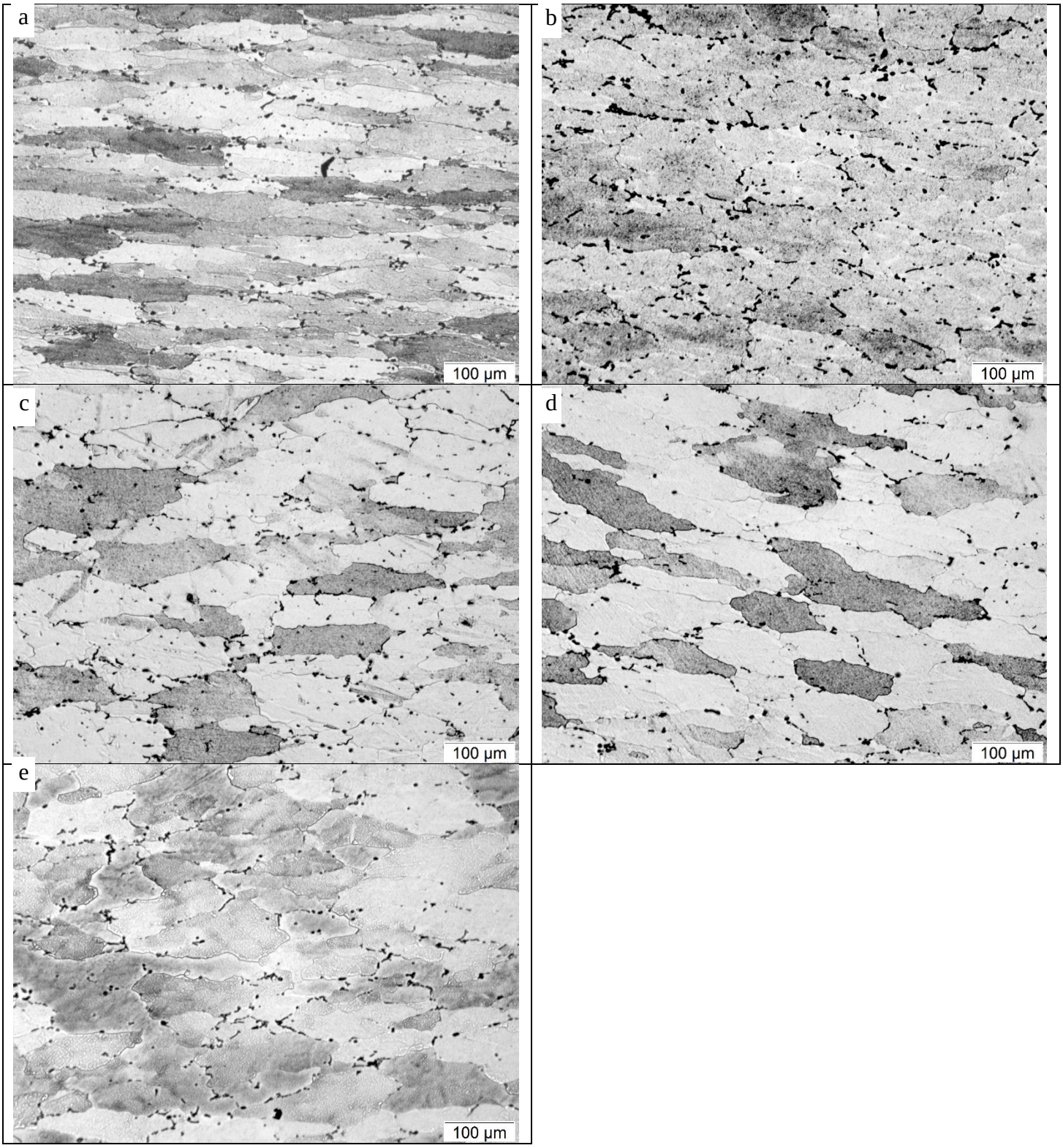

Figure 27 Optical microstructures of solution heat treated samples deformed at temperature of 500 and strain rate of 0.01 s^{-1} at SDZ position. a) after 40 min, b) after 80 min, c) after 120 min, d) after 143 min and e) after 165 min.

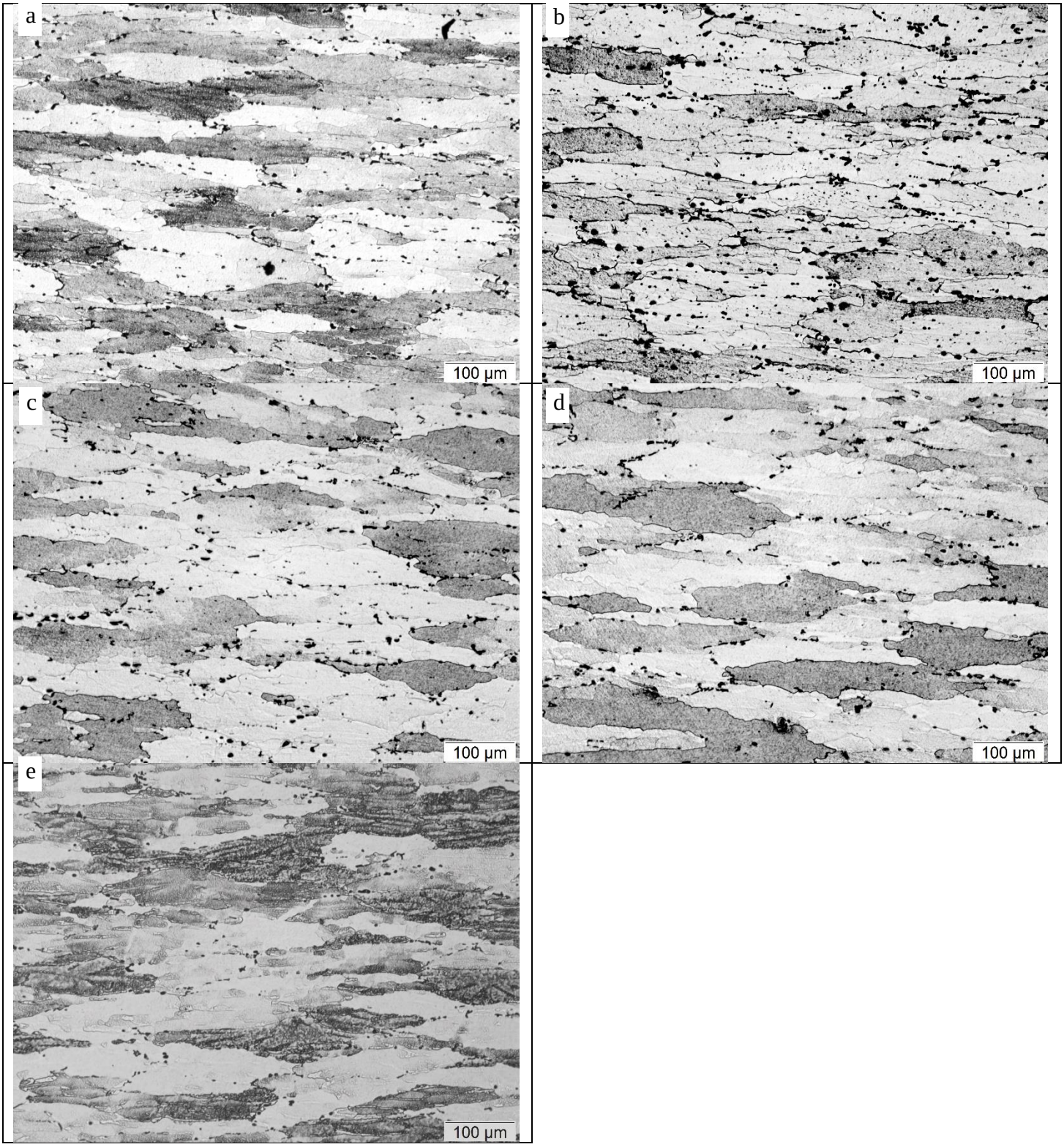

Figure 28 Optical microstructures of solution heat treated samples deformed at temperature of 500 and strain rate of 0.01 s^{-1} at MDZ position. a) after 40 min, b) after 80 min, c) after 120 min, d) after 143 min and e) after 165 min.

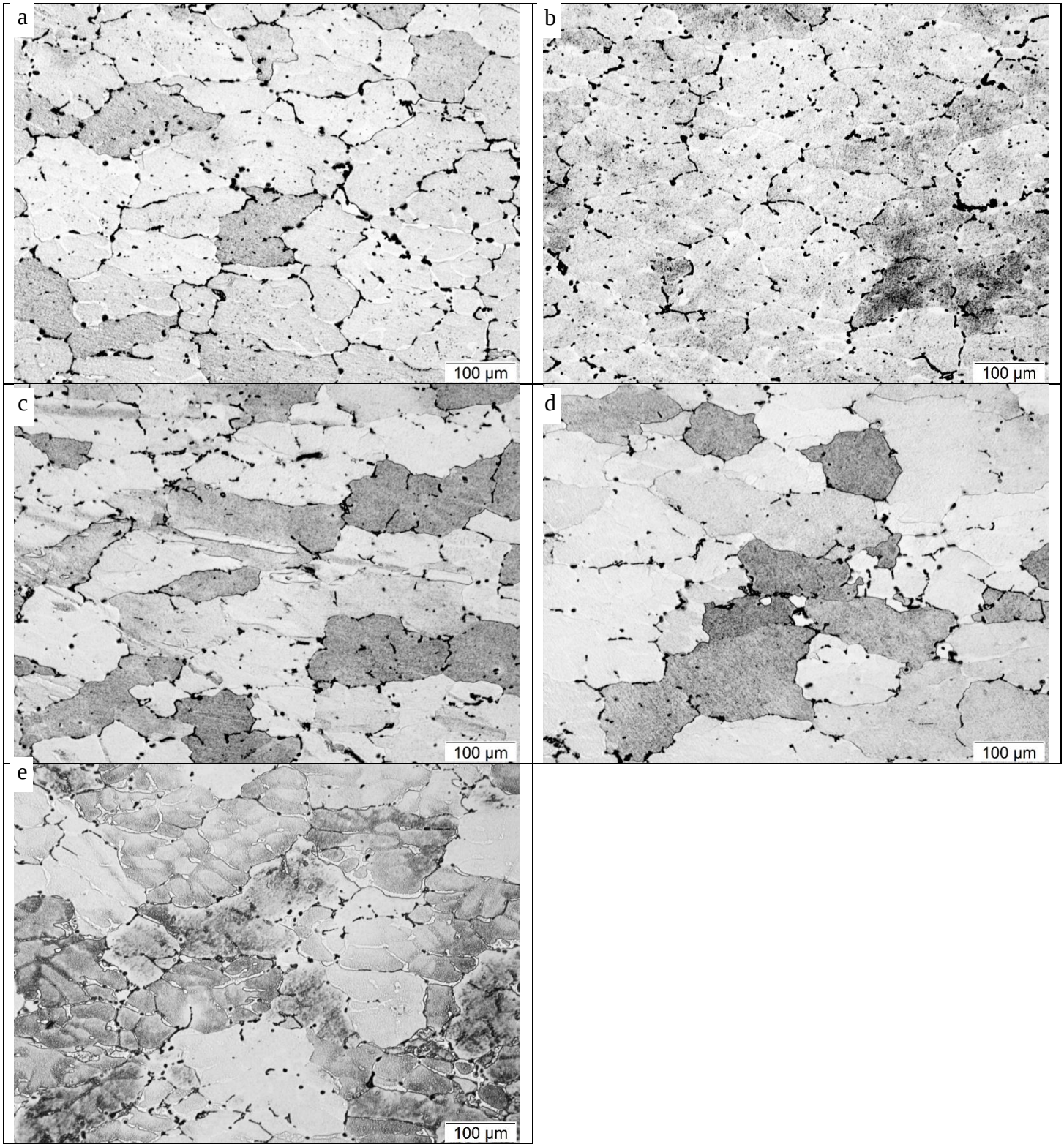

Figure 29 Optical microstructures of solution heat treated samples deformed at temperature of 500 and strain rate of 0.01 s^{-1} at DMZ position. a) after 120 min, b) after 143 min and c) after 165 min.

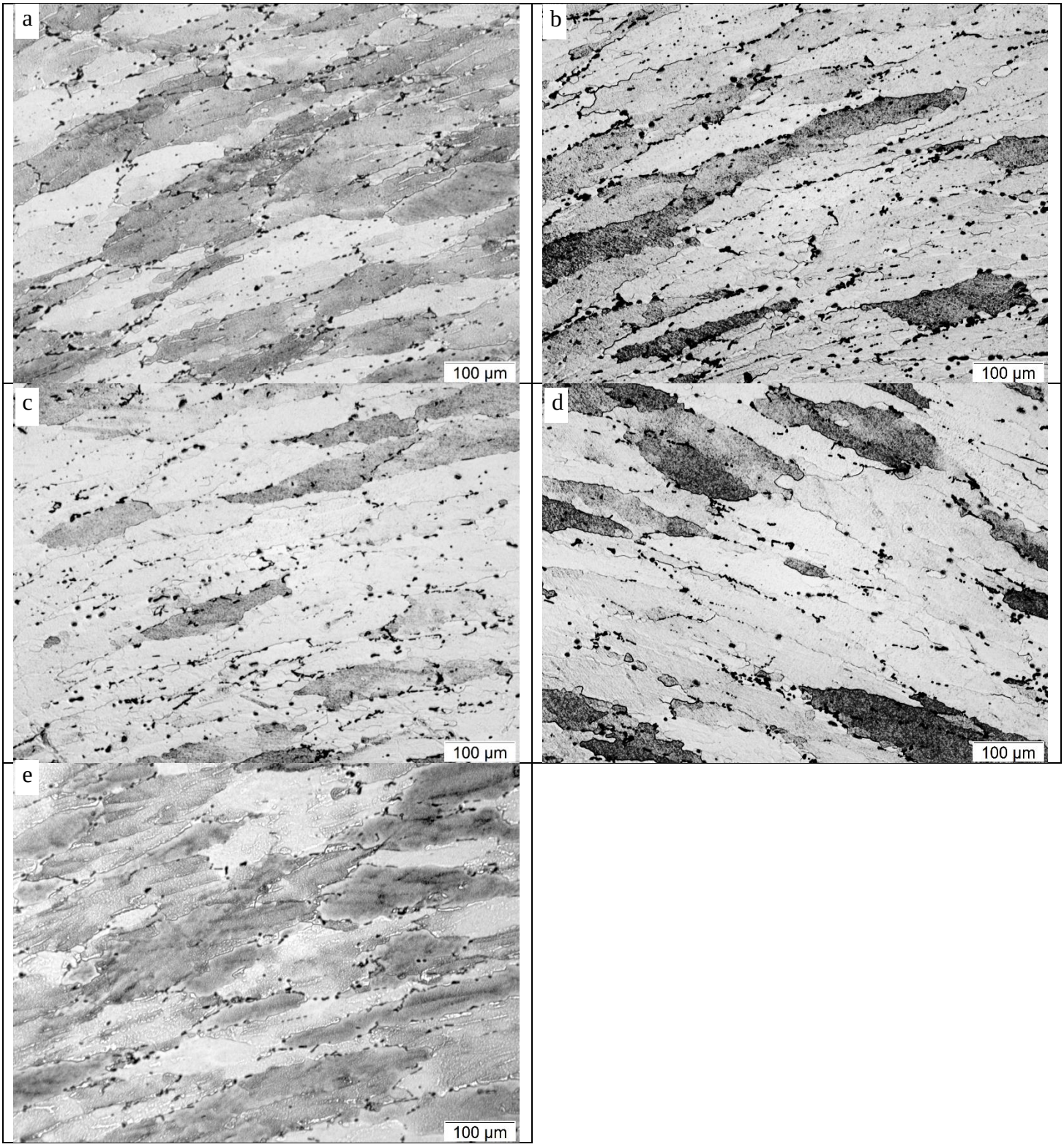

Figure 30 Optical microstructures of solution heat treated samples deformed at temperature of 500 and strain rate of 0.01 s^{-1} at TZ position. a) after 120 min, b) after 143 min and c) after 165 min.

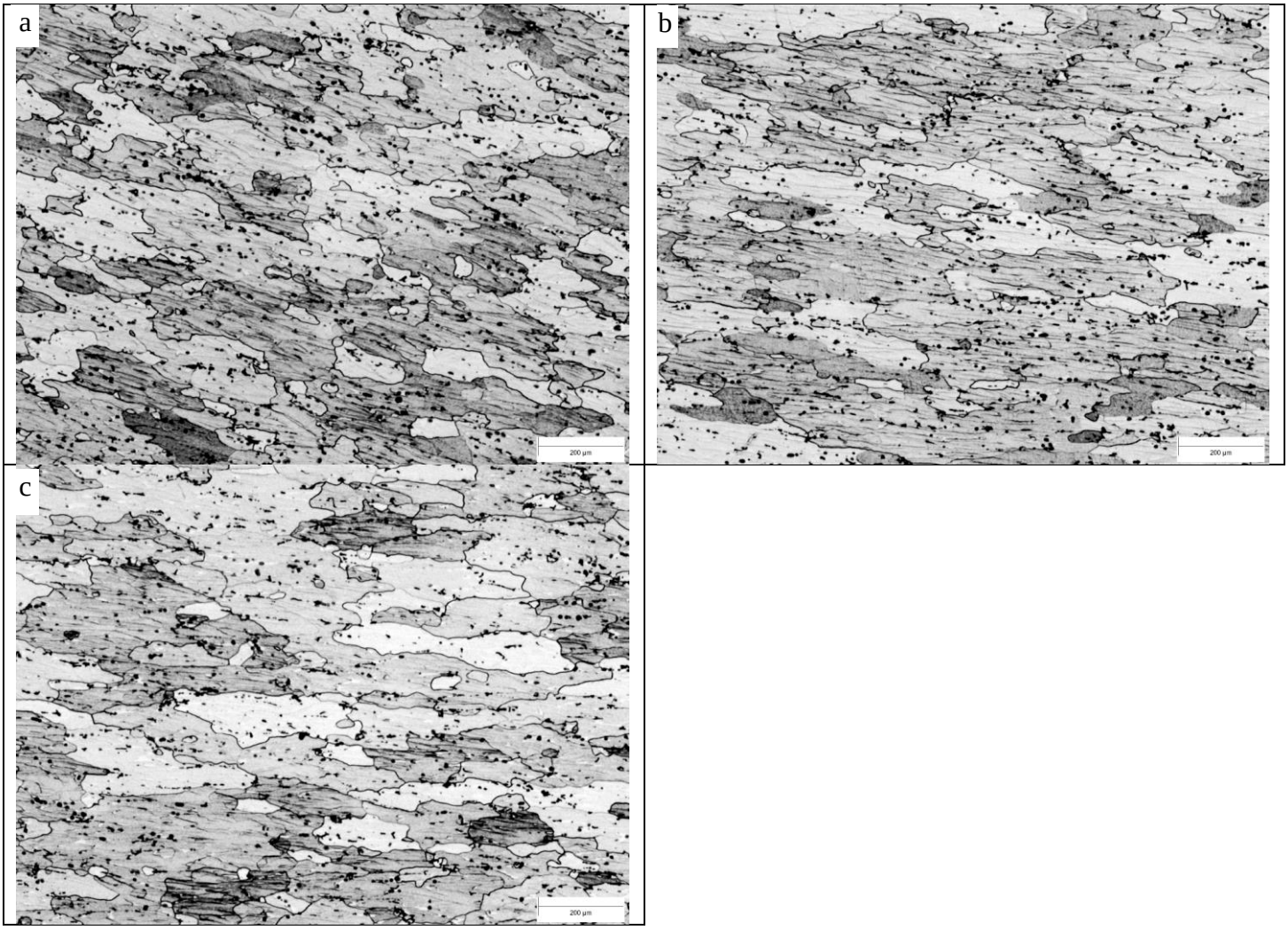

Figure 31 Optical microstructures of solution heat treated samples deformed at temperature of 350 and strain rate of 0.1 s^{-1} at MDZ position. a) after 120 min, b) after 143 min and c) after 165 min.

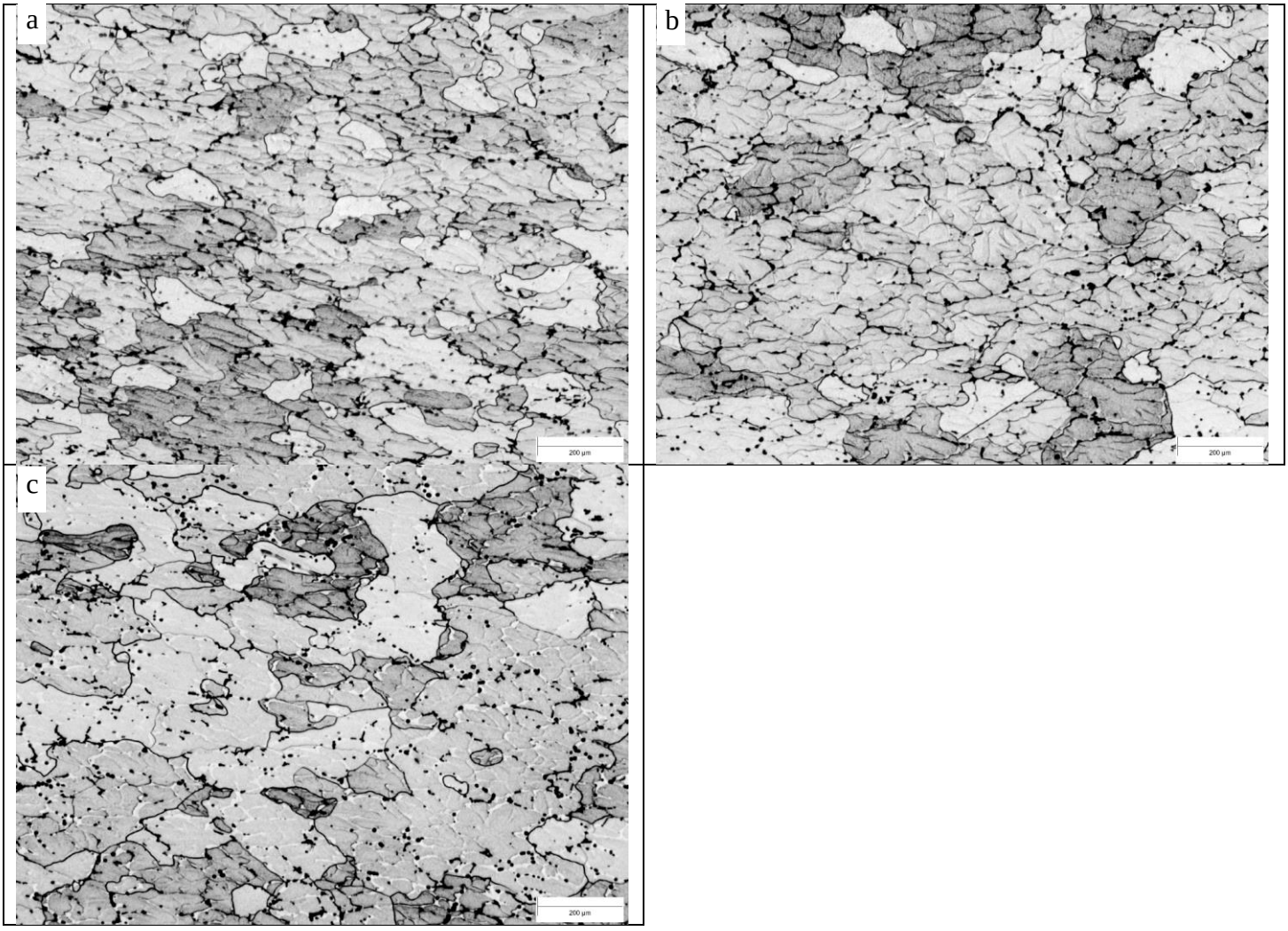

Figure 32 Optical microstructures of solution heat treated samples deformed at temperature of 350 and strain rate of 0.1 s^{-1} at DMZ position. a) after 120 min, b) after 143 min and c) after 165 min.

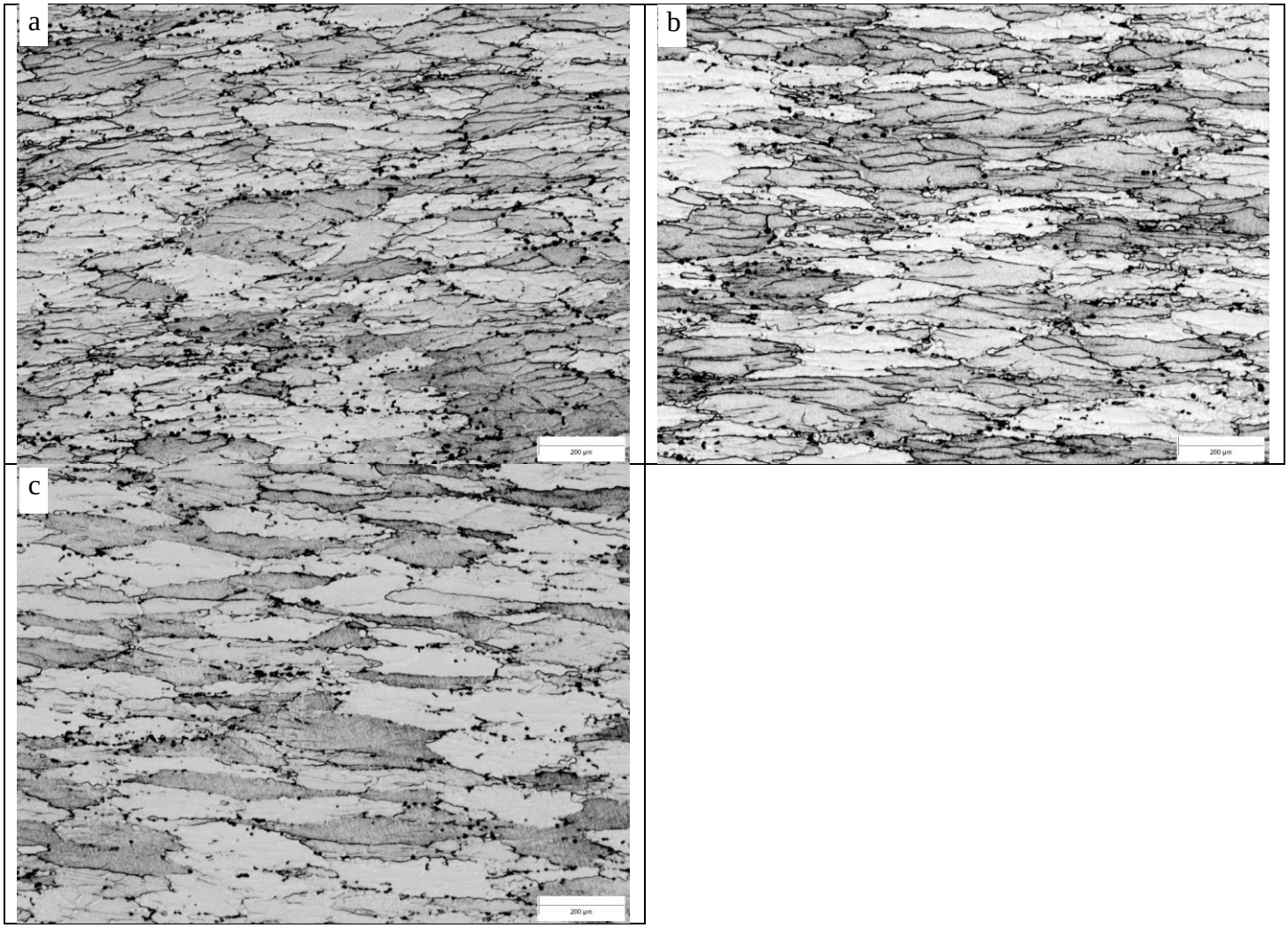

Figure 33 Optical microstructures of solution heat treated samples deformed at temperature of 500 and strain rate of 0.1 s^{-1} at MDZ position. a) after 40 min, b) after 80 min, c) after 120 min, d) after 143 min and e) after 165 min.

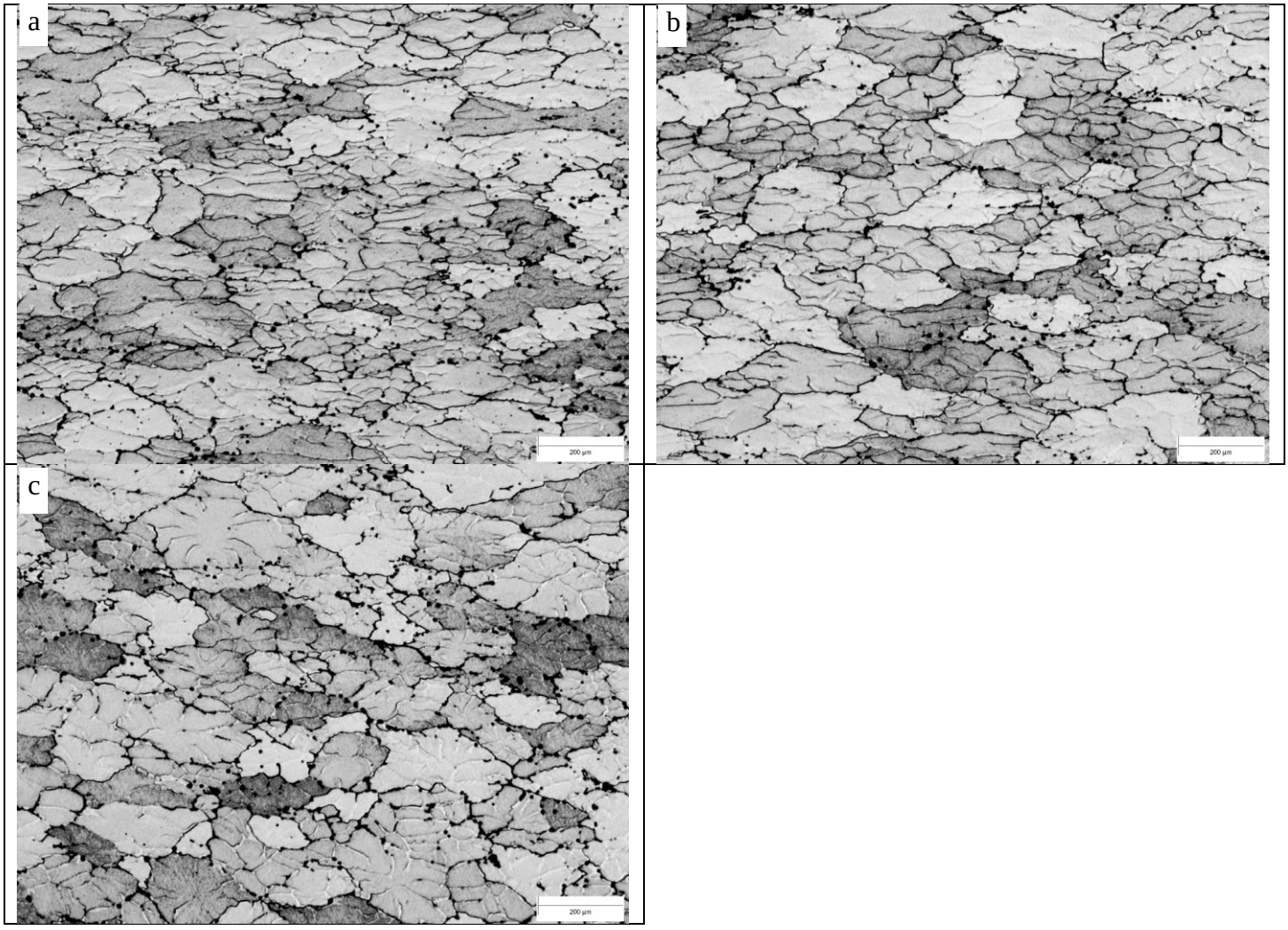

Figure 34 Optical microstructures of solution heat treated samples deformed at temperature of 500 and strain rate of 0.1 s^{-1} at DMZ position. a) after 40 min, b) after 80 min, c) after 120 min, d) after 143 min and e) after 165 min.

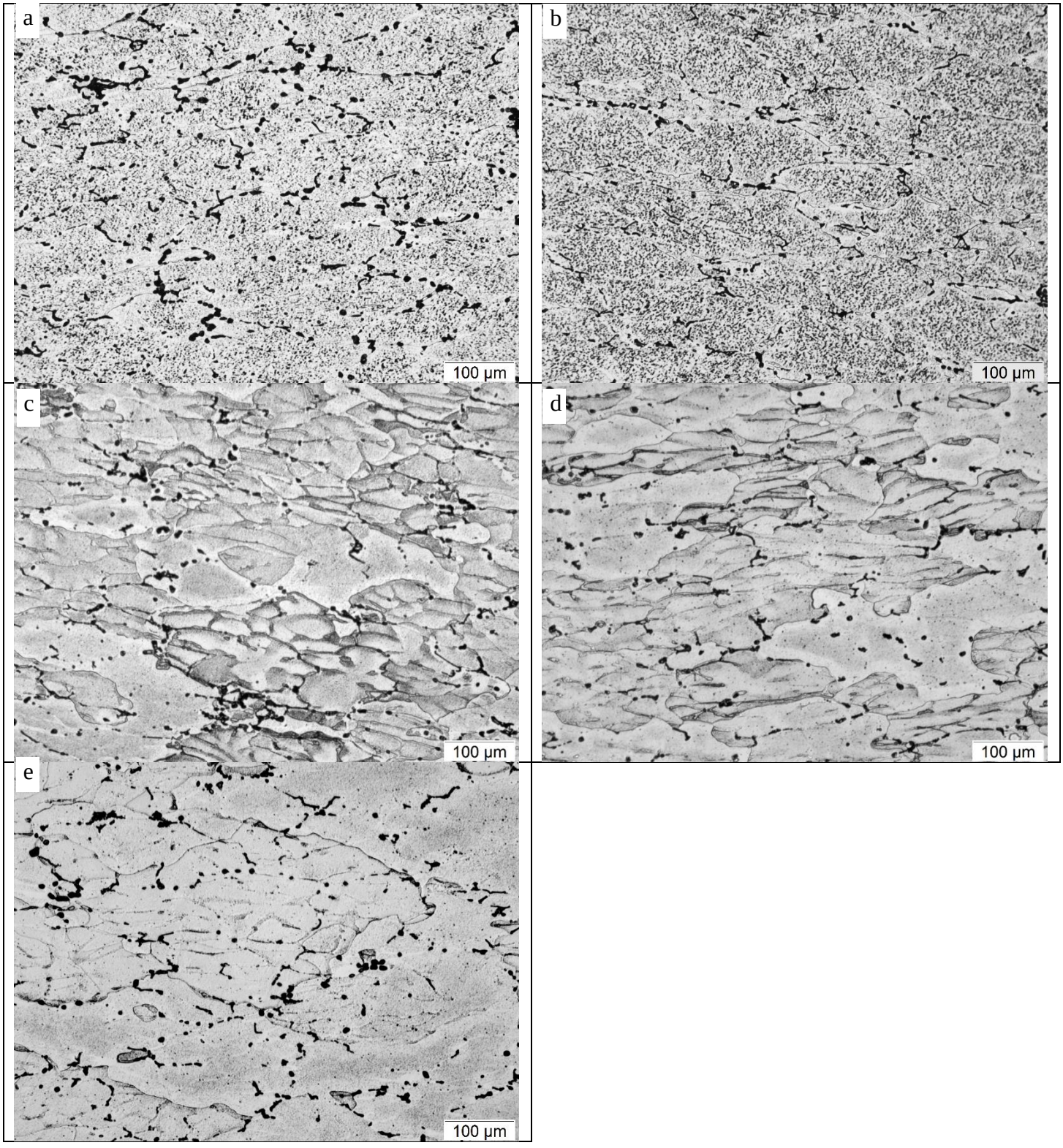

Figure 35 Optical microstructures of solution heat treated samples deformed at temperature of 350 and strain rate of 1 s^{-1} at SDZ position. a) after 40 min, b) after 80 min, c) after 120 min, d) after 143 min and e) after 165 min.

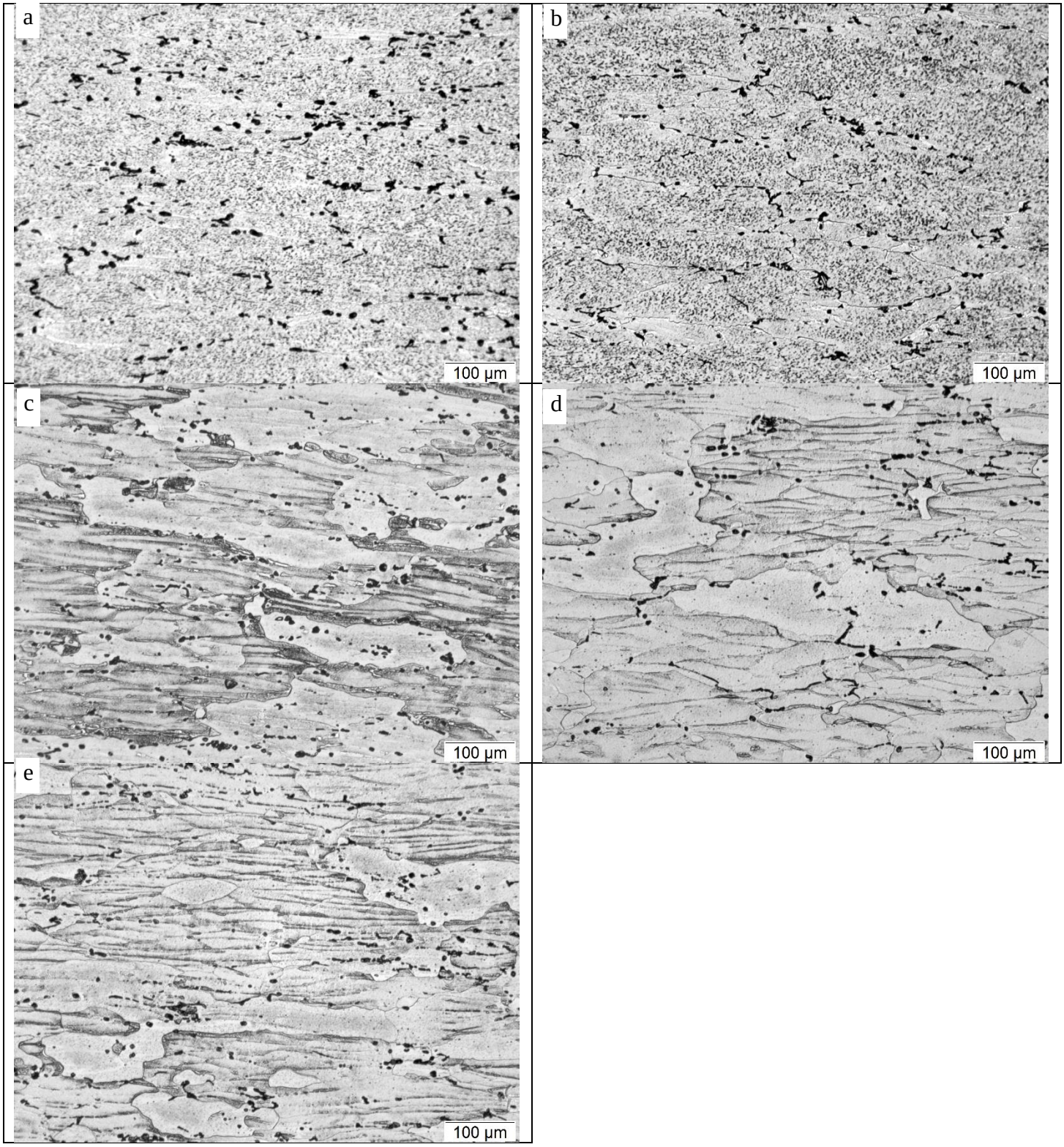

Figure 36 Optical microstructures of solution heat treated samples deformed at temperature of 350 and strain rate of 1 s^{-1} at DMZ position. a) after 40 min, b) after 80 min, c) after 120 min, d) after 143 min and e) after 165 min.

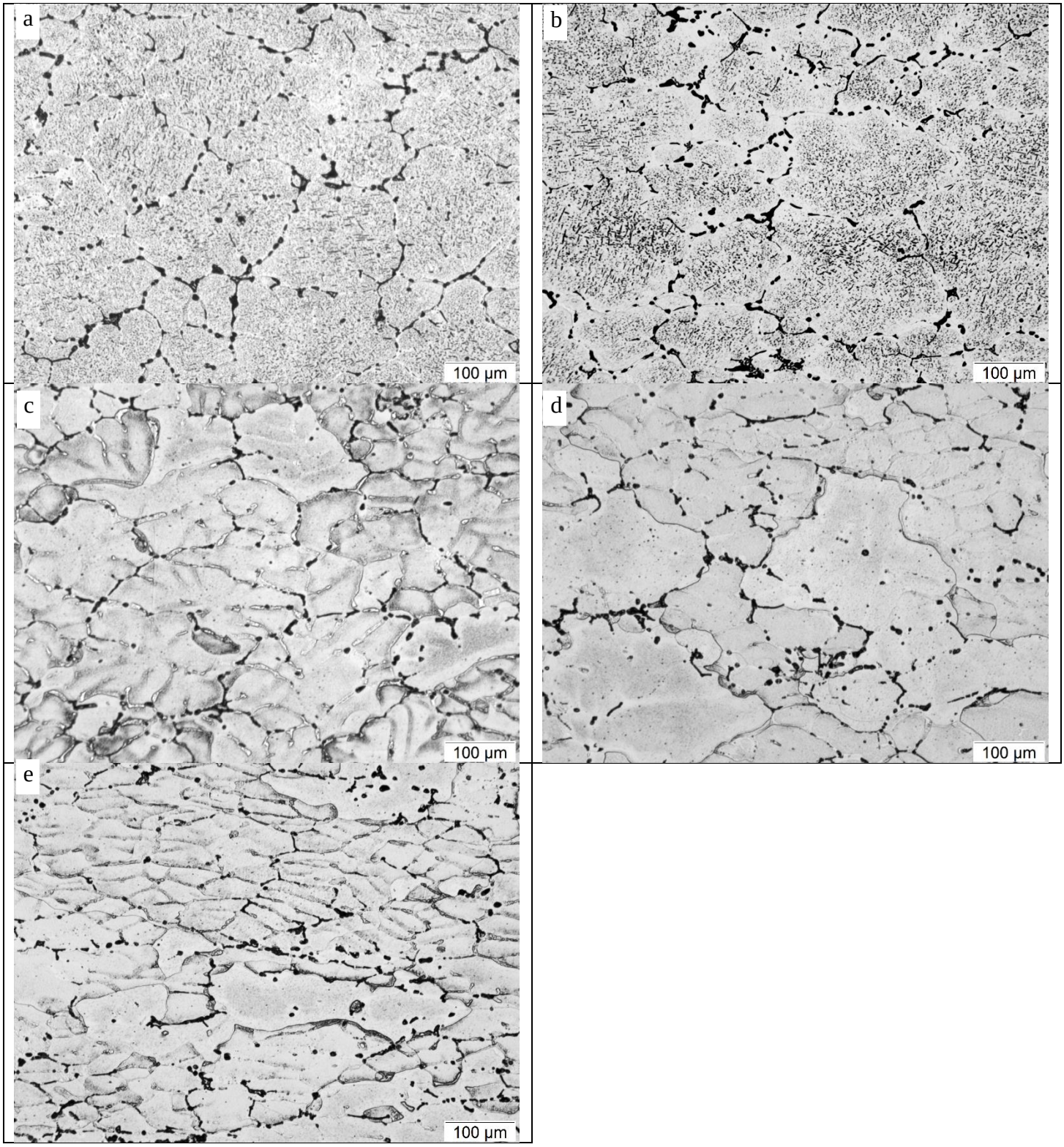

Figure 37 Optical microstructures of solution heat treated samples deformed at temperature of 350 and strain rate of 1 s^{-1} at DMZ position. a) after 40 min, b) after 80 min, c) after 120 min, d) after 143 min and e) after 165 min.

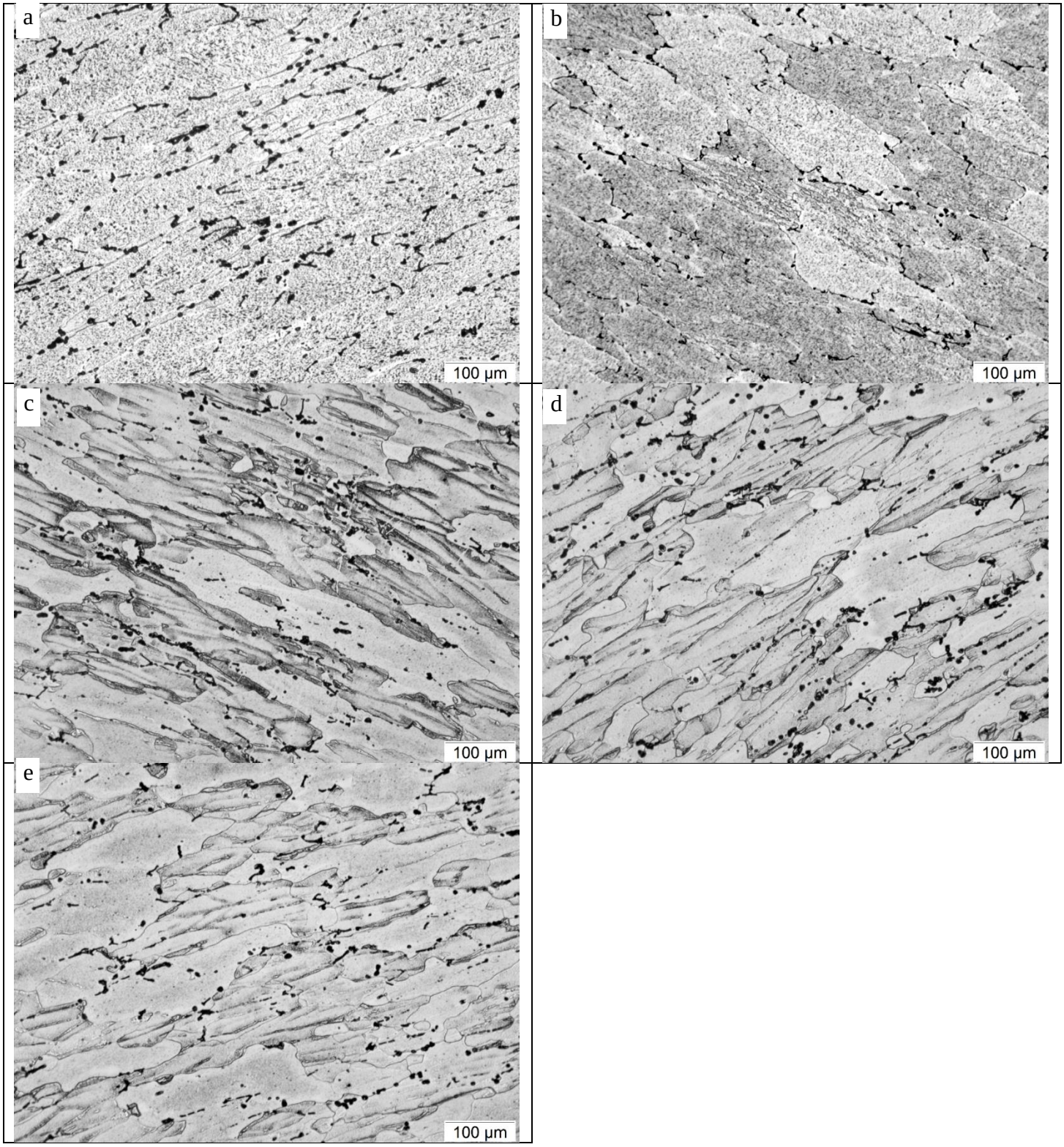

Figure 38 Optical microstructures of solution heat treated samples deformed at temperature of 350 and strain rate of 1 s^{-1} at TZ position. a) after 40 min, b) after 80 min, c) after 120 min, d) after 143 min and e) after 165 min.

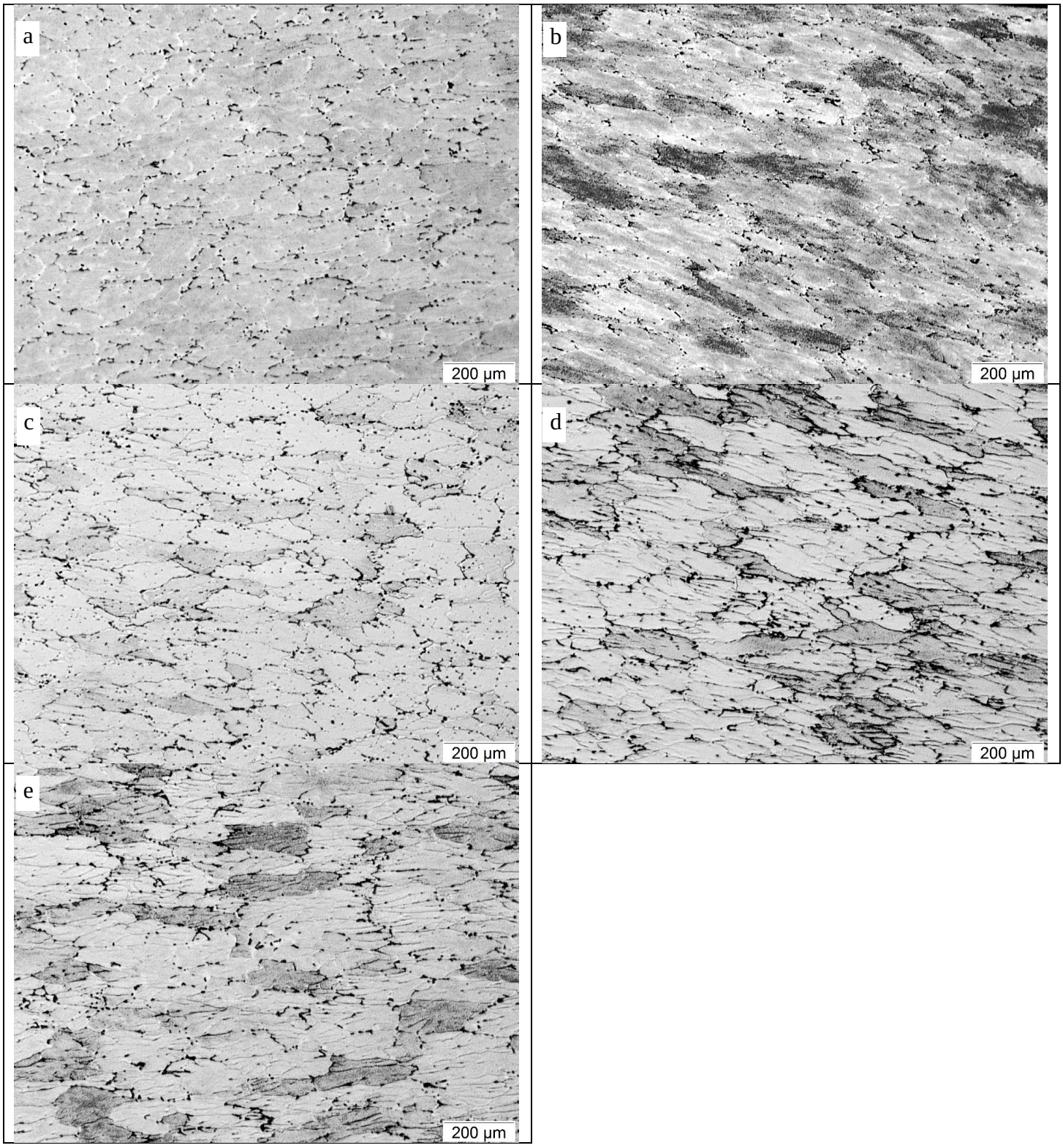

Figure 39 Optical microstructures of solution heat treated samples deformed at temperature of 500 and strain rate of 1 s^{-1} at SDZ position. a) after 40 min, b) after 80 min, c) after 120 min, d) after 143 min and e) after 165 min.

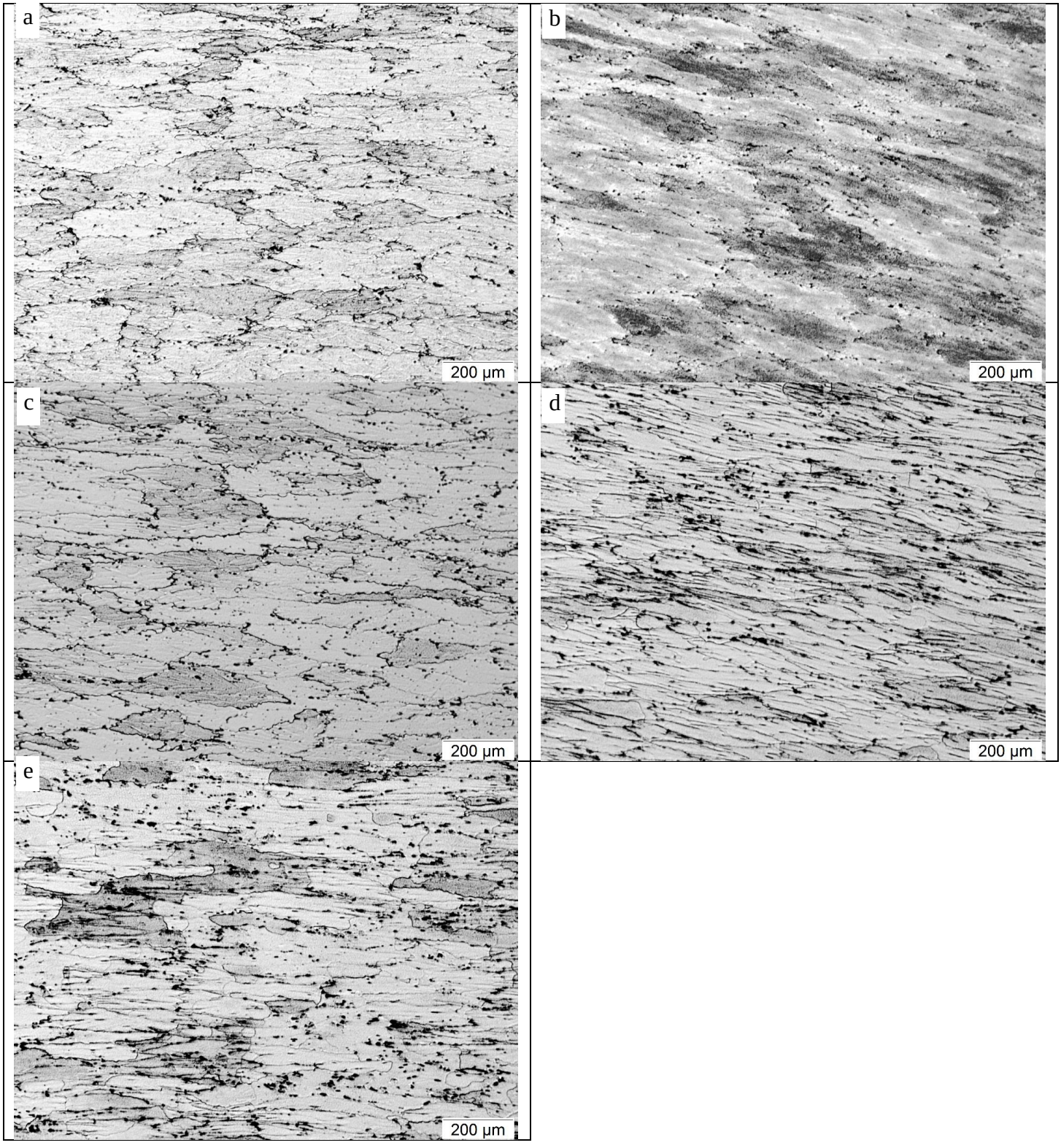

Figure 40 Optical microstructures of solution heat treated samples deformed at temperature of 500 and strain rate of 1 s^{-1} at MDZ position. a) after 40 min, b) after 80 min, c) after 120 min, d) after 143 min and e) after 165 min.

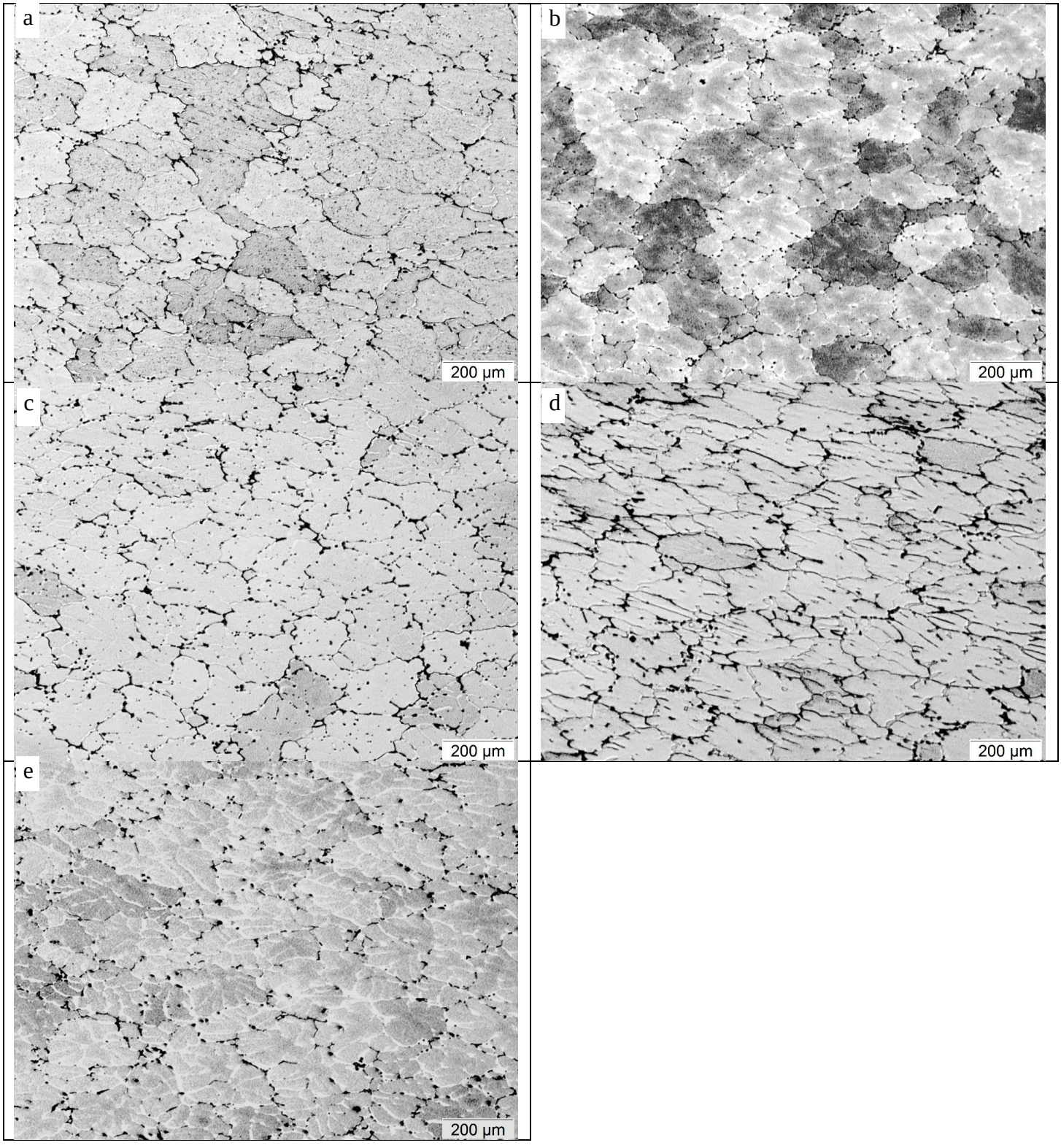

Figure 41 Optical microstructures of solution heat treated samples deformed at temperature of 500 and strain rate of 1 s^{-1} at DMZ position. a) after 40 min, b) after 80 min, c) after 120 min, d) after 143 min and e) after 165 min.

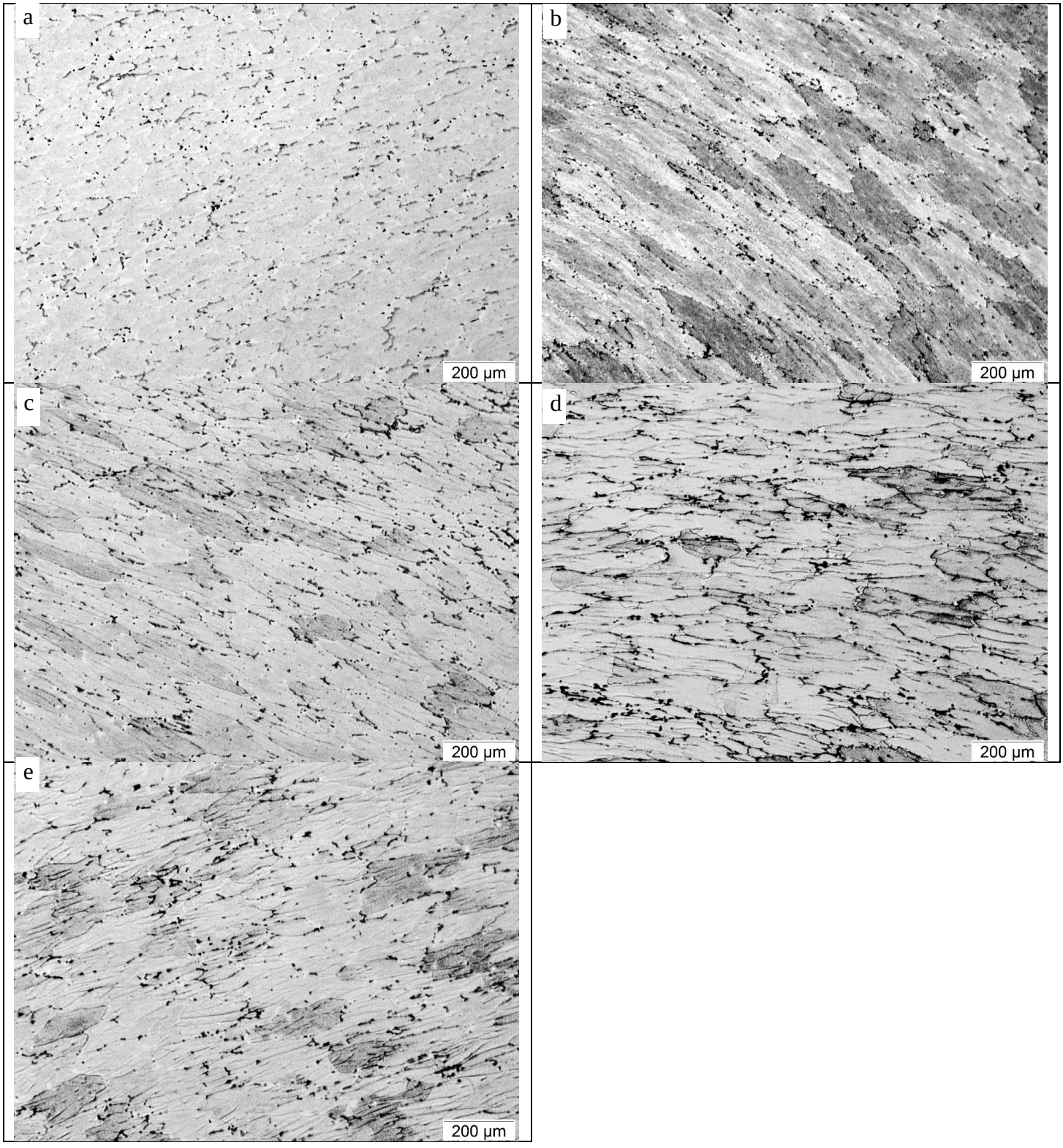

Figure 42 Optical microstructures of solution heat treated samples deformed at temperature of 500 and strain rate of 1 s^{-1} at TZ position. a) after 40 min, b) after 80 min, c) after 120 min, d) after 143 min and e) after 165 min.

5.3 SEM-BSE and EBSD Images

Scanning Electron Microscope (SEM) is a microscope that uses electron instead of light to create an image. Backscattered Electrons (BSE) is an imaging technique used to form an image of a different element sample. Whereas the element atomic number increases the image color become lighter. Figure 43 and Figure 44 show SEM-BSE images.

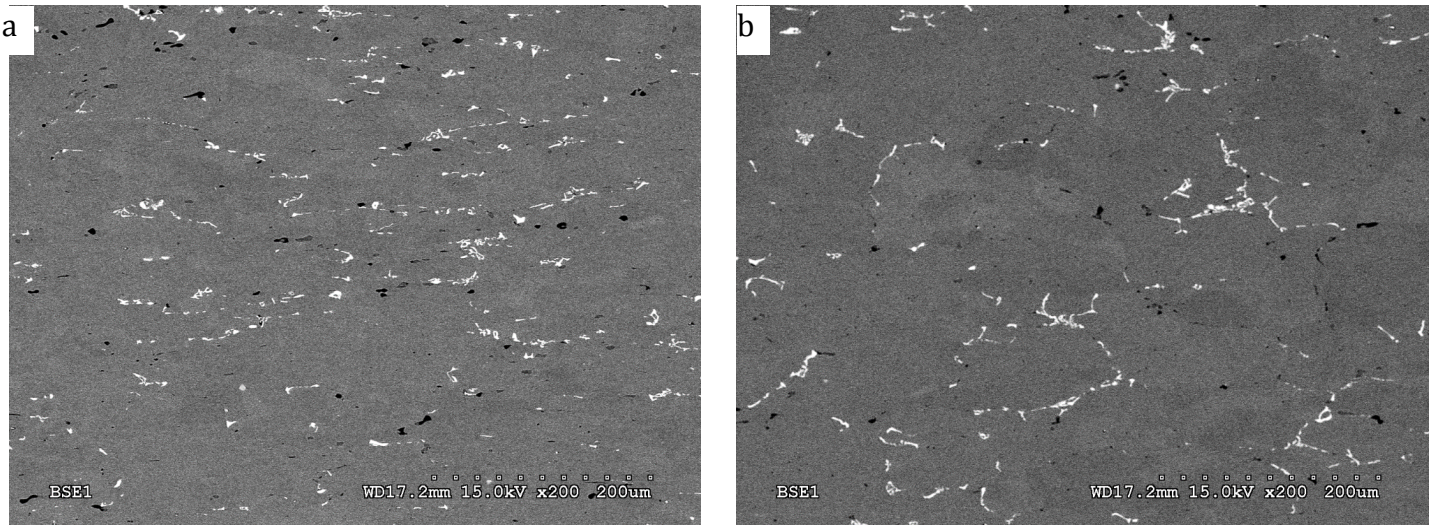

Figure 43 SEM-BSE micrograph for hot deformed sample at 0.01 s-1 & 500 ºC. a) MDZ and b) DMZ

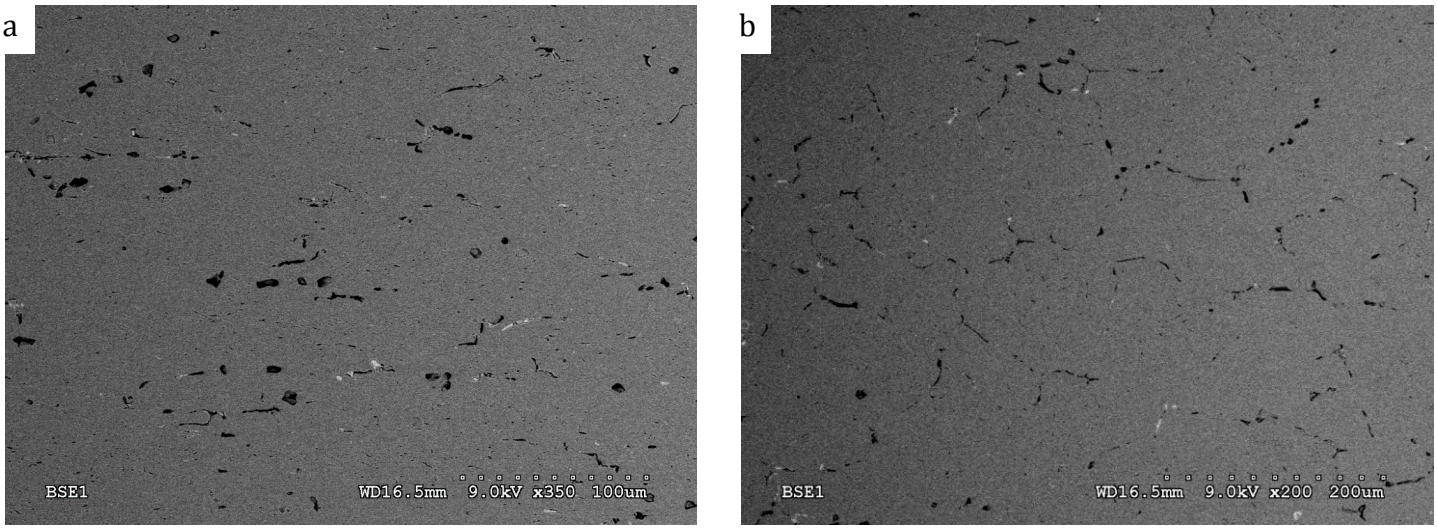

Figure 44 SEM-BSE micrograph for hot deformed sample at 1 s-1 & 350 ºC. a) MDZ and b) DMZ.

Electron backscatter diffraction (EBSD) is another technique used in SEM to study microstructural-crystallographic characterization. “EBSD provides quantitative microstructural information about the crystallographic nature of metals, minerals, semiconductors, and ceramics—in fact most inorganic crystalline materials. It reveals grain size, grain boundary character, grain orientation, texture, and phase identity of the sample under the beam”. [22] Figures from 45 to 50 present the EBSD maps for hot deformed samples at temperatures of 350 and 500 ºC for strain rates of 0.01, 0.1 and 1 s^{-1}.

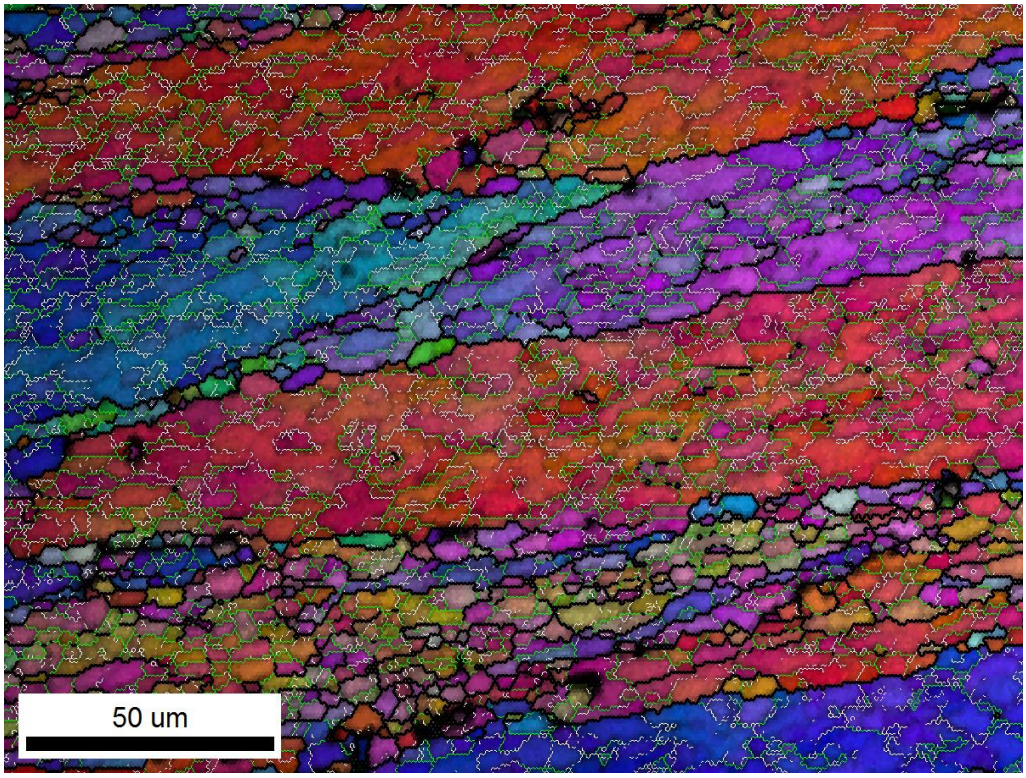

Figure 45 EBSD map of hot deformed Sample at strain rate of 0.01 s^{-1} and temperature 350ºC

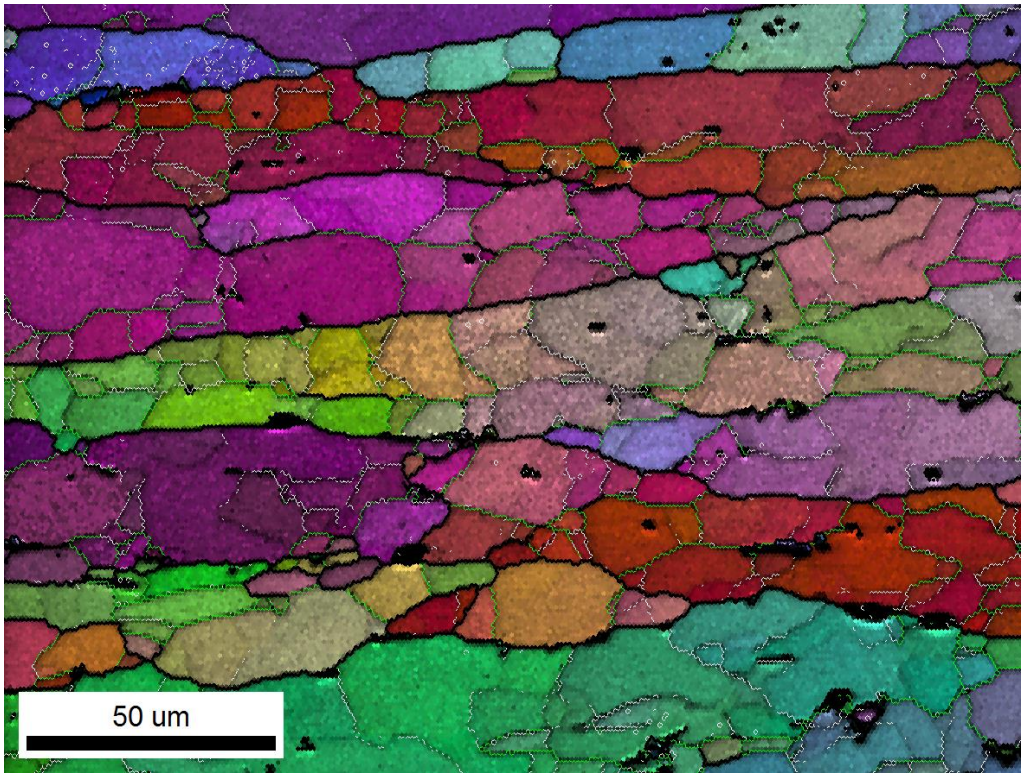

Figure 46 EBSD map of hot deformed Sample at strain rate of 0.01 s^{-1} and temperature 500ºC

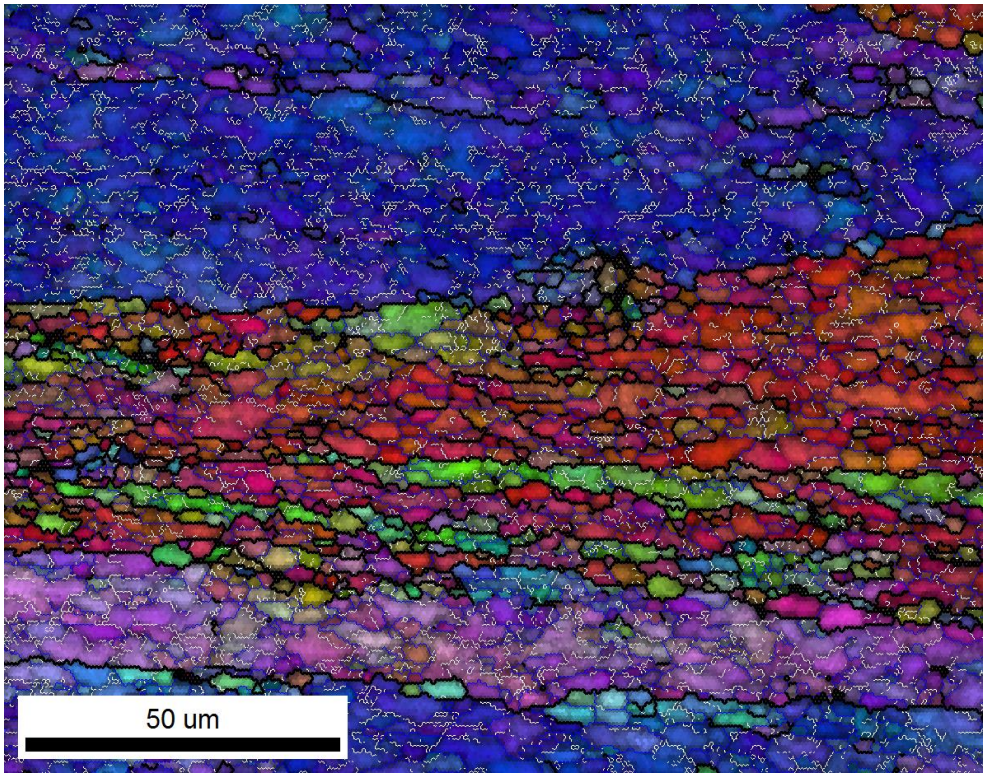

Figure 47 EBSD map of hot deformed Sample at strain rate of 0.1 s^{-1} and temperature 350ºC

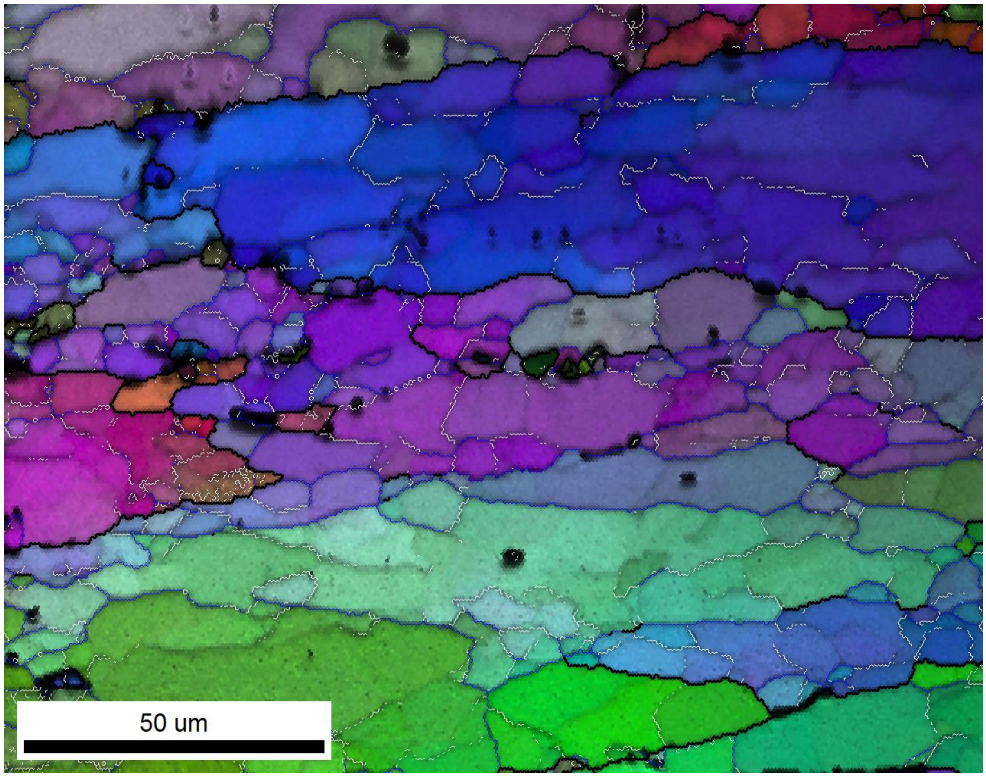

Figure 48 EBSD map of hot deformed Sample at strain rate of 0.1 s^{-1} and temperature 500ºC

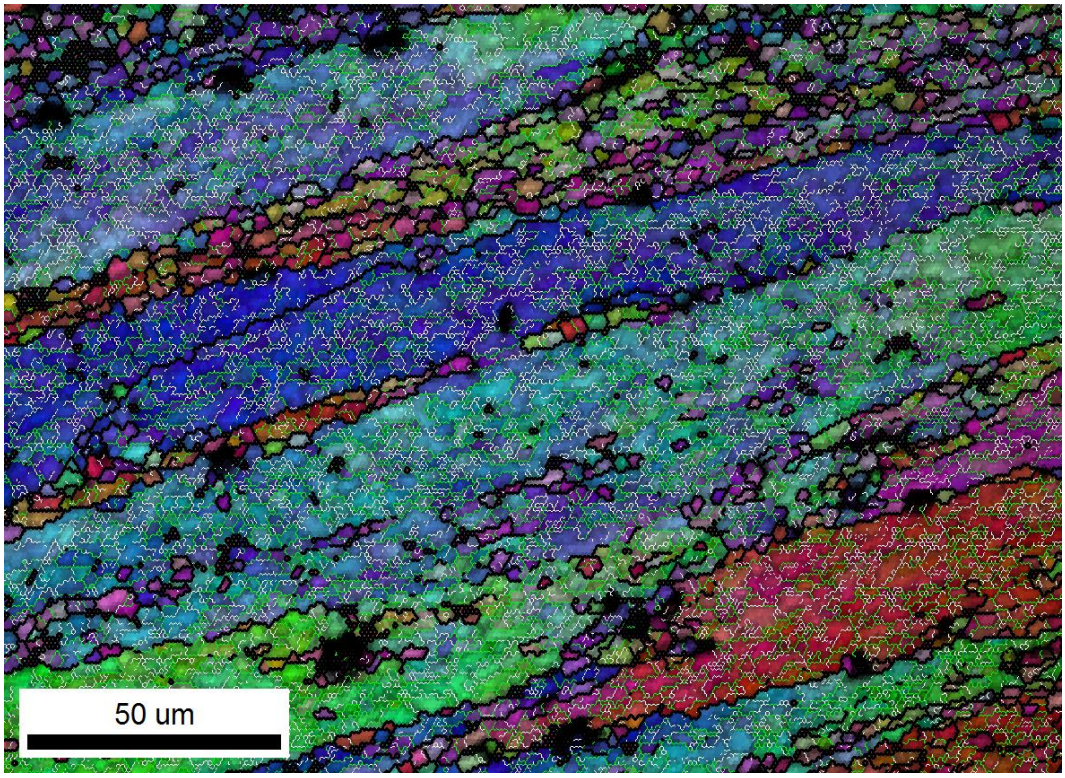

Figure 49 EBSD map of hot deformed Sample at strain rate of 1 s^{-1} and temperature 350ºC

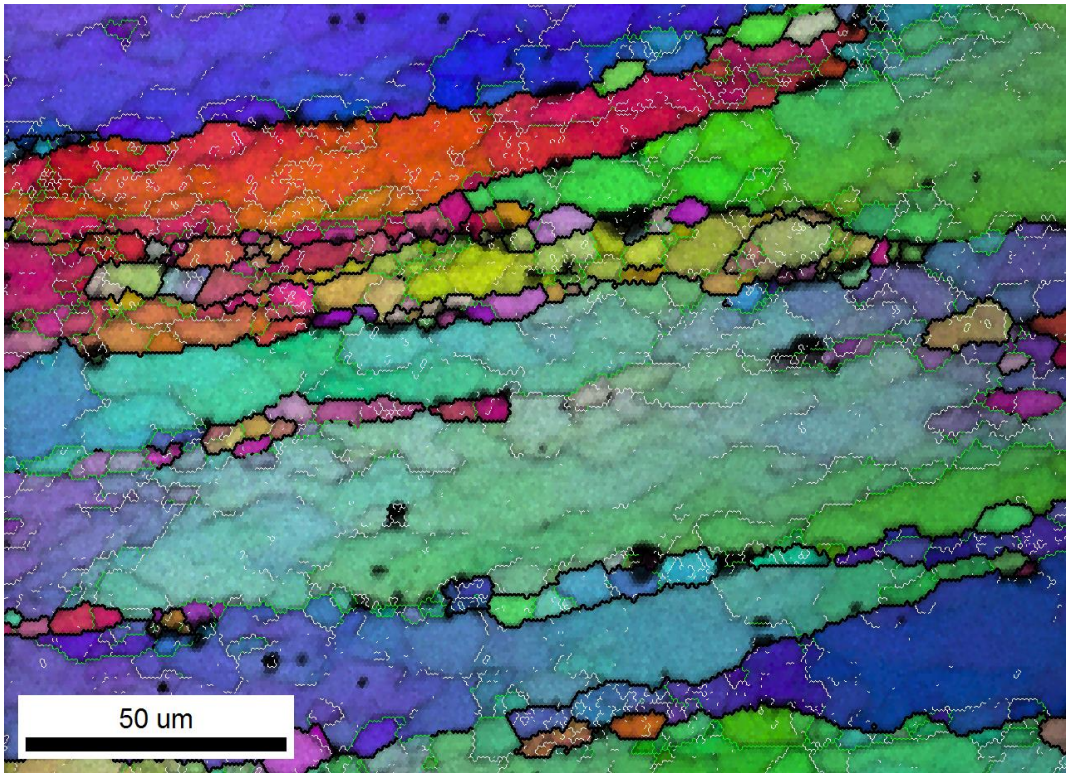

Figure 50 EBSD map of hot deformed Sample at strain rate of 1 s^{-1} and temperature 500ºC

5.4 Microindentation Hardness Testing

The hardness values of hot deformed samples at temperatures of 350 and 500 ºC for strain rates of 0.01, 0.1 and 1 s^{-1} along the line shown in Figure 17 are plotted in Figures 53.

a b

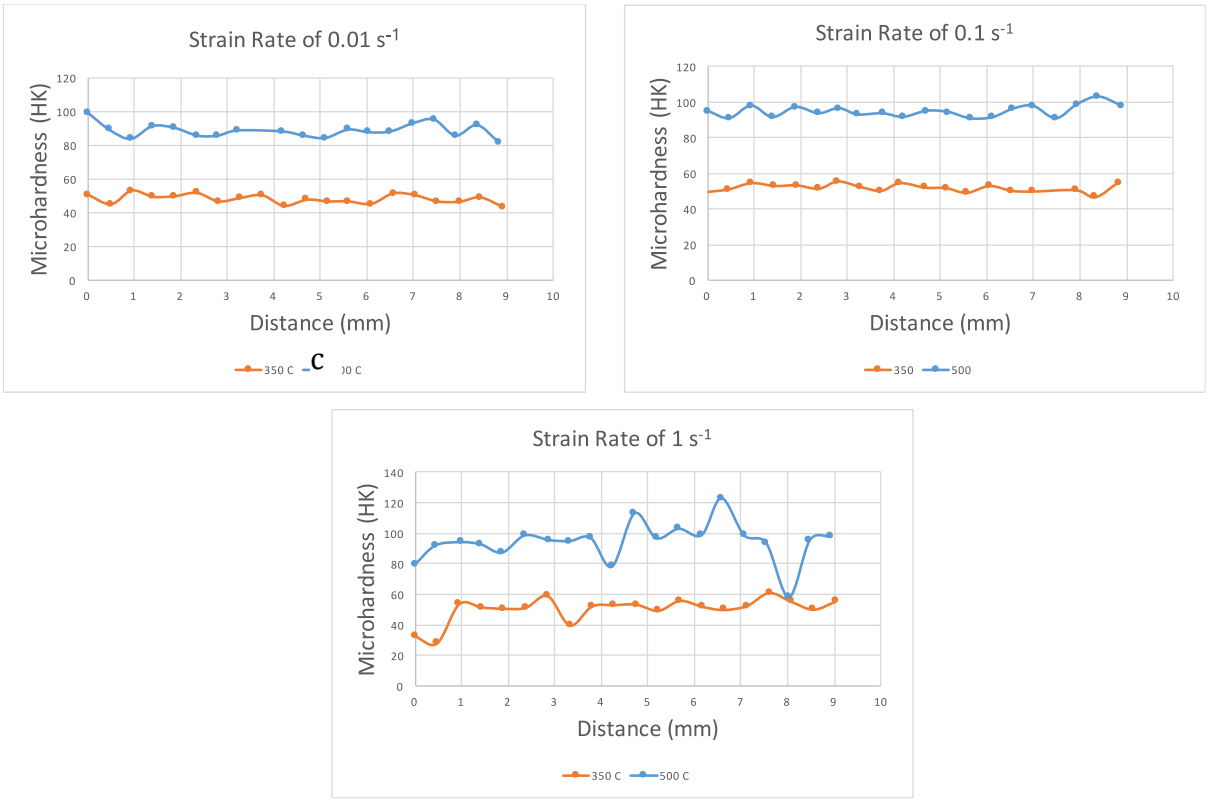

Figure 51 Microhardness taken for hot deformed samples. a) at strain rate of 0.01s^{-1}, b) at strain rate of 0.1s^{-1}, c) at strain rate of 1s^{-1}

6 DISCUSSION

6.1 Flow Stress Analysis

The flow stress curves represent material deformation behavior under certain forming conditions including eventual influence of microstructural changes especially the dynamic recovery and/or dynamic recrystallization. Figure 18 shows typical flow stress curves during hot compression deformation of aluminum alloy 6099 at strain rates of 0.01, 0.1 and 1 s^{-1} and at temperatures of 350, 400, 450 and 500 ºC. During hot deformation, the shape of flow curves is controlled by the softening mechanism;

dynamic recrystallization and/or dynamic recovery. The flow stress curves and their positions in Figure 18 depend on the temperature and strain rate. All the flow stress curves show lower stress with increasing the deformation temperature and decreasing strain rate. Under conditions of high temperature and low strain rate the flow stress curves exhibit less work hardening and more softening mechanisms (DRX or DRV).

Increasing deformation temperature results in increase in thermal energy, which offsets the work hardening and overcome the energy barriers for dislocation movement. Consequently, the dislocation density is reduced due to the enhanced dislocation movement and their annihilation at grain boundaries. Thus, increasing deformation temperature reduces the stress level and increases the dynamic softening rate since the dislocation movement resistance is reduced. In addition, decreasing strain rate results in less dislocation multiplication rate and increases the dislocation movement due to the decreasing of the tangled dislocation structures, which work as barriers for dislocation movement. Also, more time is provided for proceeding of dislocation polygonising thus the dynamic softening is increased and the stress level is reduced.[23],[24], [25]

All the flow curves show an initial rapid increase of stress with increased strain followed by slightly lower increase or its constant value or in some cases decrease of stress with strain. In the initial deformation region, the dislocations multiplied fast with increasing strain. Within this region, the work handing is a predominant mechanism and it results in a higher stress. The flow stress keeps increasing till it reaches the critical strain at the peak stress. Then, the flow will follow one of the following behaviors:

- The flow curve decreases when the dynamic softening rate is higher than the work hardening as it is observed at strain rate of 0.01, 1 s^{-1} and temperatures of 350,400 ºC, see Figure 18 a, c.

- The flow curve has steady state “plateau” when the dynamic equilibrium occurred between work hardening and dynamic softening as it is at 0.01 s^{-1} and 450,500 ºC, 1 s^{-1} and 450 ºC, see Figure 18 a, c.
- The flow curve continuously increases stress with increasing strain due to the rate of work hardening is higher than the rate of dynamic softening as it is observed at strain rate of 0.1, 1 s^{-1} and temperatures of 450,500 ºC, see Figure 18 b, c.

6.2 Microstructure Analysis

6.2.1 Undeformed Samples

In Figure 19 and Figure 20, one can see mostly equiaxed grains after deformation. In general, Lot#1 shows bigger grains, which could be due to difference in chemical composition in both Lots, especially the amount of Cr can be critical. Cr is known for retarding recrystallization and preventing the grain growth.[26] The white area along some of the grain boundary in Figure 20 is known as precipitate-free zone. It occurs uniformly throughout the entire microstructure. There are two theories, which attempt to explain this phenomenon. First and more common one is the vacancy depletion theory. The theory states that because precipitates nucleate heterogeneously on vacancies. It is well known the grain boundaries act as sink for vacancies. Thus, the area adjacent to the grain boundary shows some lack of precipitations. The second theory, which is known as the solute depletion theory states, that particles may nucleate first at the grain boundaries. These particles reduce the solute concentrations from adjacent sites and result in precipitate free zone. [27], [28]

6.2.2 Deformed Samples

It has been known that the main dynamic softening mechanism of aluminum alloys is dynamic recovery (DRV). This is due to the high stacking fault energy (SFE) of aluminum alloys, which facilitate the dislocation movements (climb and slip), which in

tern results in low stored energy to promote dynamic recrystallization (DRX). However, many researches showed evidence of DRX taking place in aluminum alloys under certain conditions. The main two types of dynamic recrystallization are known as Continuous Dynamic Recrystallization (CDRX) and Geometric Dynamic Recrystallization (GDRX). CDRX occurs when progressive accumulation of dislocation increased in low angle boundary. This forms new grains within the deformed grains. Figure 52 shows a well known example of CDRX for high purity aluminum from literature [29]. GDRX grains are formed by progressively deforming the original grains till they are pinched off to form new grains, see Figure 53. [29], [30]

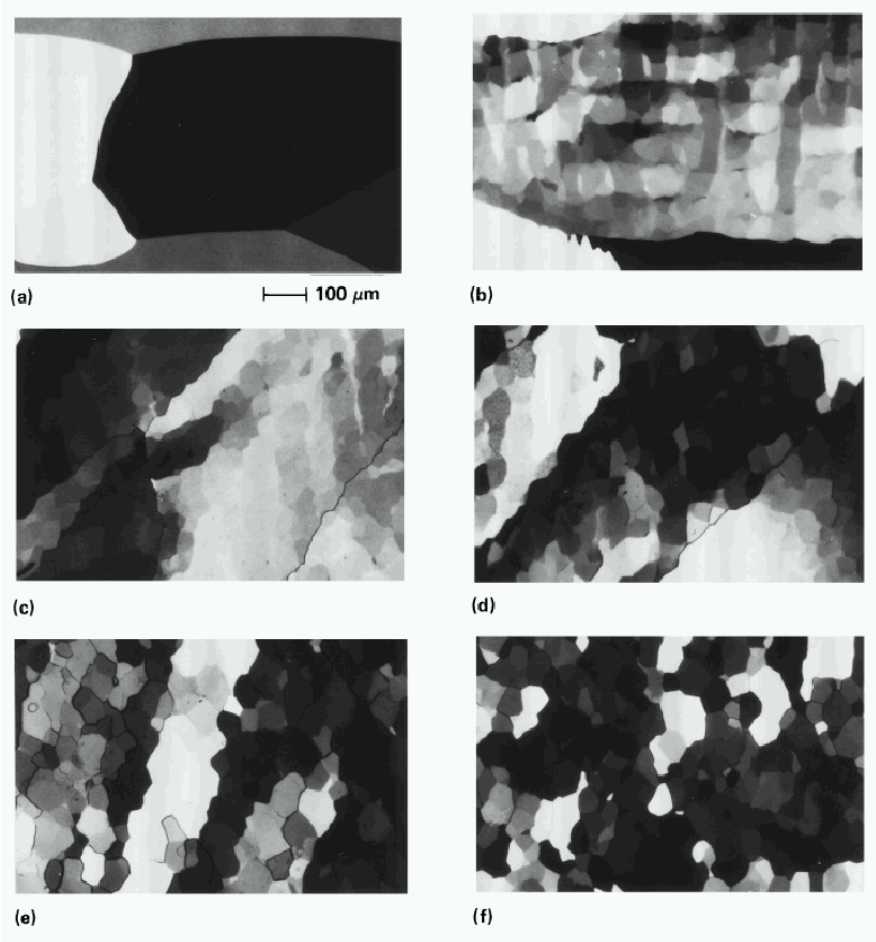

Figure 52 Represents Continuous Dynamic Recrystallization (CDRX) of high purity aluminum deformed to strains, ε: (a) 0, (b) 0.2, (c) 0.6, (d) 1.26, (e) 4.05 and (f) 16.3. [29]

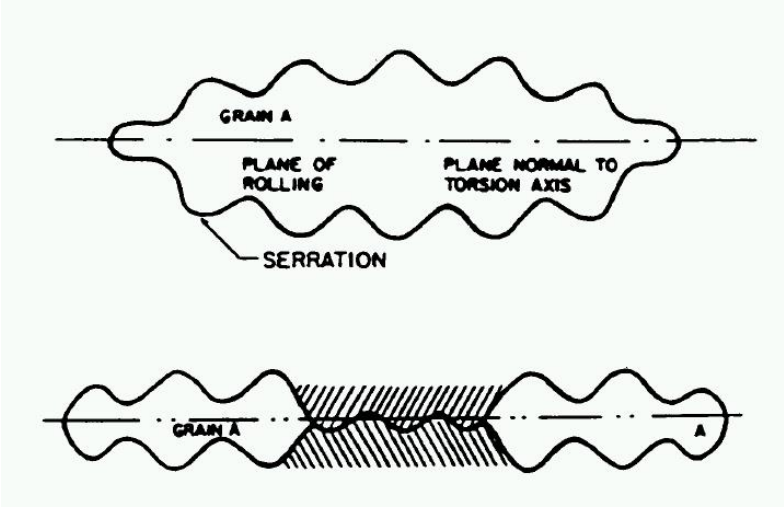

Figure 53 When the grains are elongated and thinned extremely, they pinch off where opposite serrations meet. This illustrate Geometric Dynamic Recrystallization (GDRX). [29]

Figure 21 and Figure 22 show optical micrographs of the microstructure of deformed samples at strain rate of 0.01, 0.1 and 1 s^{-1} and temperature of 350, 400 ºC in Figure 21 and 450, 500 ºC in Figure 22. In general, the optical microstructure images are not very clear because aluminum alloys are difficult to be metallographically prepared. Due the softness of the aluminum alloys and the different hardness between the matrix and intermetallics, it is challenging to reach the mirror finish surface in the polishing processes. Also, some of the hard intermetallics and other second phases are pulled out during grinding and/or polishing which results in voids, which look like overetched microstructure under the microscope but they are not. In addition, during etching process, other imperfection such as: etching pits and grain etching steps; due to uneven etching (chemical) attack to the polished surface could be formed as well. Etching pits occur due to different etching rate between the different phases in the alloy. In addition, grain etching steps exist due the different crystal orientation of each grain where each

plane is etched differentially and resulting in different light reflections and therefore colors under the microscope. [31], [32]

All optical images of microstructure were taken from the MDZ where elongated grains are observed in perpendicular to the compression direction. The grain boundaries are more pronounced as the temperature increases and the strain rate decreases. With increasing the temperature, the grain size increase and the microstructure become less homogenous. As the temperature increases or strain rate decreases some recrystallized grains were observed. At deformation conditions of 500ºC and 1 s^{-1} some grains are observed as severely elongated and broken into smaller grains as the result of the high energy forming under the conditions of the high strain rate and high temperature, see the marked ovals at Figure 22. This is an evidence of the presence of geometric dynamic recrystallization (GDRX) mechanism.

6.2.3 Solution Heat Treated Samples

During the solution heat treatment, most of the alloying elements are dissolved in a solid solution then quenched to prevent the alloying elements from precipitating out of the matrix while cooling. This heat treatment conditions form a solid solution of all the alloying elements. The optical images of microstructure and grain boundaries become more recognizable as seen in Figures from 23 to 42.

In general, all images of microstructures obtained under different strain rates show similar trend for identical temperature and locations. In other words, the microstructure of SDZ, MDZ, DMZ and TZ after 40 minutes at strain rate of 0.01 s^{-1} are comparable to the equivalent images at strain rate of 0.1 and 1 s^{-1}. No significant changes in microstructure were captured after 40 and 80 minutes samples at strain rate of 0.01 and 1 s^{-1}. So, it has been decided that only MDZ and DMZ were examined at strain rate of 0.1 s^{-1} in samples after 120, 143 and 165 minutes of solution heat treatment.

One can observe in Figures from 23 to 42 that increasing the solution heat treatment temperature increased the grains size and the dissolved alloying elements in the matrix. On the other hand, as the strain rates increased the grains size decreased due to less time available for grain growth. After applying solution heat treatment; i.e. in samples after 165 minutes, the SDZ and TZ microstructures show elongated grains to some extent with some small grains. At MDZ, the grains are severely elongated with some small recrystallized grains present. DMZ samples show the cast microstructure as expected.

In conclusion, solution heat treatment samples revealed some evidence of small grains, which could be a result of geometric dynamic recrystallization (GDRX). Additional microstructure analysis techniques, such as Electron Backscattering Diffraction Technique (EBSD) were implemented to obtain more insight into the microstructure evolution as it is discussed in the next section 6.3. Is this correct? Shouldn't it be 6.3?

6.3 BSE-SEM and EBSD Analysis

Figures 43 and 44 show electron microscopy micrographs of selected deformed sample. The grain boundaries can be distinguished by the presence of white and black needle like intermetallic. The difference in the color is due to different atomic number of elements and that is how the Backscattered Electrons technique works. The figures did not reveal any images of recrystallized grains. It could be due insufficient metallography preparation technique or because the same alloying elements exist in the matrix are available in the grain boundaries, which makes it difficult to revel the grain boundary in BSE-SEM.

Electron backscatter diffraction technique (EBSD) acquires the microstructure near the sample surface by summing the orientation of each grain or subgrain. It is a

powerful tool for microstructure characterization specially to find misorientation angles between neighboring grains and subgrains.

At strain rate of 0.01 s^{-1} and temperature 350ºC (Figure 45) some subgrains were observed with mostly misorientation angles between 1- 5 º. Also, small equiaxed high angle grain boundaries were observed as well as some elongated grains were observed. This could be an evidence of partial continuous dynamic recrystallization (CDRX) for the equiaxed high angle grain and GDRX for the elongated grains. As the temperature increased to 500º (Figure 46), most of the subgrains were recovered and some of them become grains likely due to GDRX. Also, some grain growth was observed for the recrystallized grains.

Increasing the strain rate to 0.1 s^{-1} at temperature of 350ºC (Figure 47) resulted in partial continuous dynamic recrystallized grains and subgrains. The amount of recovered subgrains by increasing the temperature (500ºC) is higher and it results in grain growth (Figure 48). Also, there is no clear evidence of recrystallization at 500ºC.

Figure 49 shows large amount of subgrains with misorientation angle from 1 – 5º and less recrystallized grains. This is due the low energy and the high strain rate of 1 s^{-1}, which does not allow enough time for recrystallization. After increasing the temperature to 500 ºC, the dominant softening mechanism here is dynamic recovery (DRV) along with evidence of equiaxed and fragmented grains as result of CDRX and GDRX respectively as shown in Figure 50.

To sum up, generally, at low temperature of 350 ºC and all strain rates, high density of subgrains and partial recrystallized grains by GDRX or CDRX mechanisms were observed. On the other hand, at high temperature of 500 ºC the dominant softening mechanism is DRV. Some evidences of recrystallized grains were observed as the energy increased; at strain rate of 0.1 and 1 s^{-1}.

6.4 Microindentation Hardness Testing

Microindentation hardness or microhardness tests were taken to evaluate the strength of each grain of the same samples used in EBSD analysis. The hardness values were compared with the values of the different grains within the same sample. A straight line pattern was used as a path for the 20 hardness measurements as shown in Figure 17. Microhardness values as a function of distance are represented in Figure 51.

There was a clear difference in hardness values between the samples processed in two different temperatures for each strain rate. However, there was not noticeable variation in hardness at each temperature at strain rate of 0.01 and 0.1 s^{-1}, see Figure 51 a and b. At high strain rate, some hardness variation was observed for 350 and 500ºC as shown in Figure 51c.

The difference in hardness between 350 and 500ºC is due to the solid solution. While more alloying elements are dissolved at higher temperature and they do strengthen the sample. The lower hardness at strain rate of 1 s^{-1} could be an indicator of recrystallized grains. To verify that, two other microhardness tests were taken in the vicinity of the sample edge of the hot deformed sample at strain rate of 1 s^{-1} and temperature 500ºC. The same procedure was used twice; two straight lines and both parallel to the compression direction were applied. Figure 54 shows that both edges indicated low hardness around the distance of 4 mm in the middle of the test distance. It is known that highest deformation value is expected to be present in the middle of hot deformed sample according to performed FEM analysis, which results are presented in Figure 55. The lower hardness indicates less dislocation density. This emphasizes that some grains have been recovered or recrystallized.

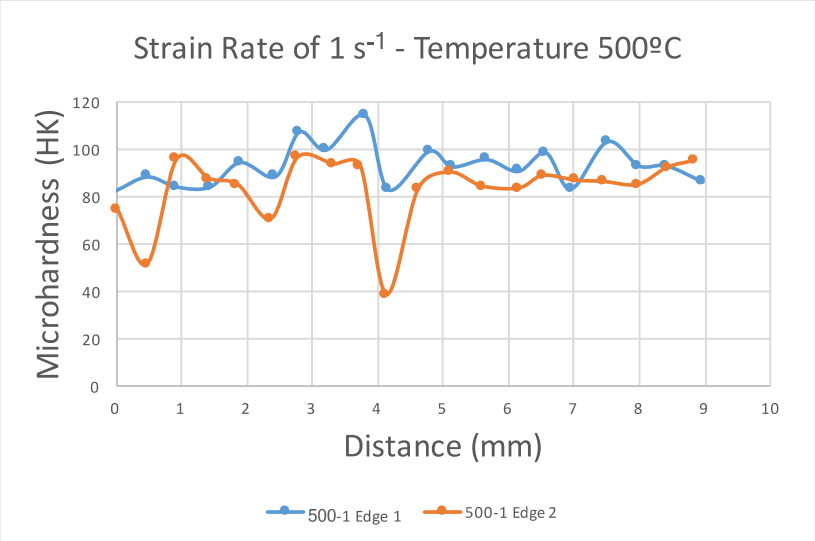

Figure 54 Microhardness taken for hot deformed sample at strain rate of $1s^{-1}$ and temperature 500ºC.

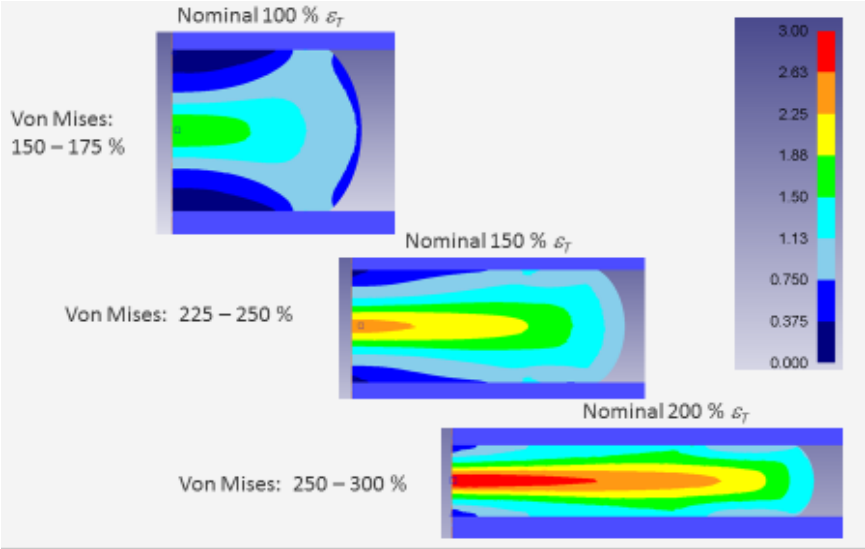

Figure 55 FEM shows strain (deformation) distribution of the hot deformed sample. [20]

7 CONCLUSIONS

The research objective of this project was to understand the microstructure development of newly developed aluminum alloy 6099 during hot forging and subsequent heat treatment process. The idea was to hot deform a small-scale samples mimicking the industrial deformation condition on the thermo-mechanical simulator – Gleeble 3500. The hot compression experiments have been performed at different strain

rates of 0.01, 0.1 and 1 s^{-1} and temperatures of 350, 400, 450 and 500 ºC. The corresponding observation based on the results obtained from different characterization techniques can be summarized as follow:

- Based on the performed hot compression studies the classical true stress – true strain curves were obtained. In general, the flow stress increases with decreasing deformation temperatures and/or increasing strain rate.
- All flow stress exhibited rapid increasing at the beginning of deformation due to dislocation multiplication. Once the flow stress reached the peak stress, some samples exhibited slight flow stress increase, some remained unchanged with typical “plateau” behavior and some showed decrease in stress.
- Micrographs obtained using the Light Optical Microscopy revealed elongated grains in all hot deformed samples. As the temperature increased or strain rate decreased, some recrystallized grains were observed. Also, increasing the temperature and strain rate make the microstructure became less homogenous and the grain size increased. Sever or localized deformation conditions were seen at high strain rate of 1 s^{-1}.
- During solution heat treatment of hot deformed samples, different deformation zones were investigated and the results were listed for each one:
    - SDZ and TZ, the microstructures showed elongated grains with some small grains as recrystallized grains.

- MDZ after 165 min, the grains have severely elongated with some small grains as GDRX grains.
- DMZ, as cast microstructure.

- At high temperature (500 ℃), EBSD maps did not show any evidence of recrystallized grain at strain rate of 0.01 s^{-1}. However, some GDRX/CDRX revealed at strain rate of 0.1 and 1 s^{-1}. Thus, the dominant softening mechanism seems to be the dynamic recovery (DRV) and partial dynamic recrystallization at higher energy.
- Also, EBSD maps showed that partial GDRX or CDRX took place at low temperature of 350 ℃ and strain rate of 0.01, 0.1 and 1s^{-1}.
- In addition, some grain growth was observed at 500ºC compared to the 350ºC at all strain rates.
- Microhardness data did not reveal significant variation in mechanical properties between samples processed at strain rate of 0.01 and 0.1 s^{-1}. However, some low hardness values were shown at strain rate of 1 s^{-1} supporting hypothesis that some recrystallized grains do occur, mainly at high temperature where grain growth took place.

8 Future Work

The performed research was not able to answer all the important scientific questions. Future follow up studies can be suggested as follows;

- Develop a physical and numerical model by using the results of this study.
- Force-stroke diagrams were captured and can be analyzed to get more insight into the hot compression mechanisms.

- Experimental study can be performed on the effects of the adiabatic heating during the hot compression tests at different temperatures and stain rates.
- Understand and analyze the grain size changes with respect to different isothermal holding time.
- Since aluminum alloys are sensitive to forging temperature, more hot compression tests can be conducted at small temperature intervals between 350 – 450 ºC.
- Transmission electron microscopy (TEM) can be used to identify the dispersoids/precipitates, which inhibit recrystallization during hot deformation and solution heat treatment. [33] Also, analyzing the dislocation movements behavior to understand the softening mechanisms.
- Study the distribution of alloying elements within the grains by electro-probe microanalyzer (EPMA).

REFERENCES

[1] H. Nagaumi, Y. Takeda, S. Pongsukiwat, and T. Umeda, “Hot Tear and its Prevention of Irregular Near Net Shape D . C . Billet of High Strength Al-Mg-Si Alloy.”

[2] Kalpakjian and Schmid, *Manufacturing Engineering and Technology*, 5th ed. Pearson Education India, 2001.

[3] M. G. Rathi and N. a Jakhade, “An Overview of Forging Processes with Their Defects,” *Int. J. Sci. Res. Publ.*, vol. 4, no. 6, pp. 1–7, 2014.

[4] M. Hirscvogel and H. v. Dommelen, “Some applications of cold and warm forging,” *J. Mater. Process. Tech.*, vol. 35, no. 3–4, pp. 343–356, 1992.

[5] A. M. and R. N. K. Siegert, “Forging Alloys,” 1994.

[6] D. Siegert, K., Ringhand, “Designing of Forgings,” 1994.

[7] R. Palin, V. Johnston, S. Johnson, A. D’Hooge, B. Duncan, and J. I. Gargoloff, “The Aerodynamic Development of the Tesla Model S - Part 1: Overview,” 2012.

[8] G. W. Kuhlman, “Forging of aluminum alloys.,” *ASM Handb.*, vol. 14, pp. 241–254, 1988.

[9] S. Semiatin, “ASM Handbook, Vol. 14: Forming and Forging,” *ASM Int.*, vol. 14, p. 483, 1993.

[10] “Ladish Preparing For World’s Largest Isothermal Press.” [Online]. Available: http://forgingmagazine.com/feature/ladish-preparing-worlds-largest-isothermal-press. [Accessed: 21-May-2017].

[11] “How are forgings produced | Forging Industry Association.” [Online]. Available: https://www.forging.org/forging/how-are-forgings-produced.html. [Accessed: 21-May-2017].

[12] J. Dossett and G. Totten, “Steel Heat Treating Fundamentals and Processes,” 2013.

[13] G. Weeks, “Aluminium car wheels: Manufacturing, materials & design considerations,” no. 2012.

[14] “Alcoa Wheels North America -- Alcoa Wheel; Truck Wheels; Aluminum Wheels; Lightweight Wheel.” [Online]. Available: http://www.arconic.com/alcoawheels/north_america/en/info_page/home.asp. [Accessed: 15-May-2017].

[15] “APP Forged Wheels & Center Discs.”

[16] S. J. Andersen, H. W. Zandbergen, J. Jansen, C. TrÆholt, U. Tundal, and O. Reiso, “The crystal structure of the β″ phase in Al–Mg–Si alloys,” *Acta Mater.*, vol. 46, no. 9, pp. 3283–3298, 1998.

[17] A. H. Geisler and J. K. Hill, “Analyses and Interpretations of X-ray Diffraction Effects in Patterns of Aged Alloys,” *Acta Crystallogr.*, vol. 1, pp. 233–252, 1948.

[18] C. D. Marioara, S. J. Andersen, J. Jansen, and H. W. Zandbergen, “Atomic model for GP-zones in a 6082 Al-Mg-Si system,” *Acta Mater.*, vol. 49, no. 2, pp. 321–328, 2001.

[19] L. Preserve, “Claves , Steven R . Characterization and Analysis of the Localized Deformation of 6xxx Aluminum Alloy Extrudates June 2002,” 2002.

[20] *Courtesy of Nick Nanninga from Accuride. Received by private communication on 05/30/2016. .*

[21] J. R. Davis, J. R. D. & Associates, and A. I. H. Committee, “Aluminum and aluminum alloys,” p. 796, 1993.

[22] T. Maitland and S. Sitzman, “EBSD technique and materials characterization examples.pdf,” *Scanning Microsc. Nanotechnology. Tech. Appl.*, pp. 41–76, 2007.

[23] C. Shi, J. Lai, and X. Chen, “Microstructural Evolution and Dynamic Softening Mechanisms of Al-Zn-Mg-Cu Alloy during Hot Compressive Deformation,” pp. 244–264, 2014.

[24] Q. Guo-zheng, “Characterization for Dynamic Recrystallization Kinetics Based on Stress-Strain Curves,” *Recent Dev. Study Recryst.*, pp. 61–64, 2013.

[25] E. McQueen, H. J., Spigarelli, S., Kassner, M. E., & Evangelista, *Hot Deformation and Processing of Aluminum Alloys*, vol. 20111578. CRC Press, 2011.

[26] “How and why alloying elements are added to aluminum.” [Online]. Available: http://www.alcotec.com/us/en/education/knowledge/qa/How-and-why-alloying-elements-are-added-to-aluminum.cfm. [Accessed: 04-Jun-2017].

[27] H. K. D. H. Bhadeshia, “Precipitate free zones.” [Online]. Available: https://www.phase-trans.msm.cam.ac.uk/abstracts/pfz.html. [Accessed: 04-Jun-2017].

[28] Y. Minamino, Y. Koizumi, N. Tsuji, S. Hirosawa, T. Sato, C. Hin, E. Bobruk, I. Sabirov, V. Kazykhanov, and T. Ogura, “Quantitative characterization of precipitate free zones in Al–Zn–Mg(–Ag) alloys by microchemical analysis and nanoindentation measurement,” *Sci. Technol. Adv. Mater*, vol. 5, 2004.

[29] R. D. Doherty, D. a. Hughes, F. J. Humphreys, J. J. Jonas, D. Juul Jensen, M. E. Kassner, W. E. King, T. R. McNelley, H. J. McQueen, and a. D. Rollett, “Current issues in recrystallization: A review,” *Mater. Today*, vol. 1, no. 2, pp. 14–15, 1998.

[30] W. Z. Misiolek and W. R. Van Geertruyden, “Combined Numerical Simulation and Microstructure Characterization for Prediction of Physical Properties in Extruded Aluminum Alloys,” *Key Eng. Mater.*, vol. 424, pp. 1–8, 2009.

[31] G. F. Vander Voort, *Metallography: Principles and practice*. 1985.

[32] H. Zhu, X. Zhang, M. Couper, and A. Dahle, "The Formation of Streak Defects on Anodized Aluminium Extrusions," *J. Miner. Met. Mater. Soc.*, vol. 62, no. 5, pp. 46–51, 2010.

[33] X. Y. Lü, E. J. Guo, P. Rometsch, and L. J. Wang, "Effect of one-step and two-step homogenization treatments on distribution of Al3Zr dispersoids in commercial AA7150 aluminium alloy," *Trans. Nonferrous Met. Soc. China (English Ed.*, vol. 22, no. 11, pp. 2645–2651, 2012.

VITA

Mohammed Alamoudi was born in Jeddah, Saudi Arabia. He is the son of Tariq Alamoudi and Lolulua Alamoudi. In 2004, he graduated from the high school and started to study mechanical engineering at King Abdulaziz University (KAU), Jeddah. In 2010, he graduated with a Bachelor of Science Degree in Mechanical Engineering. Right after that, he moved to Riyadh and joined King Abdulaziz City for Science and Technology (KACST) as scientific researcher at the National Center for Advanced Materials Technology. In 2013, he has been assigned as deputy director of the National Center for Non-Destructive Testing. In mid of 2014, he was granted a scholarship from KACST to the USA to continue his graduate studies. He joined graduate school at Lehigh University. Mohammed was awarded his Master of Science Degree in Materials Science and Engineering from Lehigh University in summer of 2017.